Central Aromatic Ring Substitution on Non-Fullerene Acceptors Boosts Performance of Organic Photovoltaics

Ruibin Bian[a], Xiangjian Cao[a], Zhaoyang Yao*[,a], Wenkai Zhao[b], Shuhui Ding[a], Guankui Long[b], Xiangjian Wan*[,a], Chenxi Li[a], Yongsheng Chen*[a]

[a] State Key Laboratory and Institute of Elemento-Organic Chemistry, The Centre of Nanoscale Science and Technology and Key Laboratory of Functional Polymer Materials, Renewable Energy Conversion and Storage Center (RECAST), Frontiers Science Center for New Organic Matter, College of Chemistry, Nankai University, Tianjin, 300071, China.

[b] School of Materials Science and Engineering, National Institute for Advanced Materials, Renewable Energy Conversion and Storage Center (RECAST), Nankai University, Tianjin, 300350, China.

Corresponding E-mails: yschen99@nankai.edu.cn; zyao@nankai.edu.cn; xjwan@nankai.edu.cn.

Materials.

Polymeric donor PM6 was purchased from Woerjiming (Beijing) Technology Development Institute, respectively. All the other reagents and chemicals were purchased from commercial suppliers and were used directly without further purification unless otherwise noted. The overall synthesis route and detailed synthesized procedures of CH-Ph and CH-Th and the corresponding characterizations were displayed in "Synthesis section." below.

^{1}H and ^{13}C nuclear magnetic resonance (NMR) spectra.

The ^{1}H (400MHz) and ^{13}C (101MHz) nuclear magnetic resonance (NMR) spectra were taken on a Bruker AV400 Spectrometer.

High-Resolution Mass Spectra (HR-MS).

The High-Resolution Mass Spectra (HRMS) were recorded by Solarix scimax MRMS with high-resolution matrix-assisted laser desorption/ionization (HR-MALDI).

Ultraviolet-Visible (UV-vis) Absorption.

UV-Vis spectra were obtained by a Cary 5000 UV-Vis spectrophotometer. The spin coater (Brand-REESEEN，PvS-mini7) used in the lab is from Jiangyin J. Wanjia Technology Co., Ltd.

Cyclic voltammogram (CV).

The CV experiments were performed with a LK98B II Microcomputer-based Electrochemical Analyzer. All measurements were conducted at room temperature with a three-electrode configuration. Among them, a glassy carbon electrode was employed as the working electrode, a saturated calomel electrode (SCE) was used as the reference electrode, and a Pt wire was used as the counter electrode. Tetrabutylammonium phosphorus hexafluoride (n-Bu_4NPF_6, 0.1 M) in acetonitrile was employed as the supporting electrolyte, and the scan rate was kept at 100 mV s $^{-1}$. Electrochemically

reversible ferrocene was employed as internal reference. The HOMO and LUMO energy levels were calculated from the onset oxidation and the onset reduction potentials, respectively, by following the equation E_{HOMO} = -(4.80+$E_{ox\ onset}$) eV, E_{LUMO} = -(4.80+$E_{re\ onset}$) eV.

Differential Scanning Calorimetry (DSC) and Thermal Gravimetric Analyzer (TGA).

DSC and TGA measurements were performed on a TG209 DSC204 DMA242 METTLER3+ DSC instrument with a heating rate of 10 °C min^{-1} under a nitrogen atmosphere.

Computational Methods in This Work.

All alkyl chains were replaced with methyl groups (-CH_3) to reduce the computational requirements. The structures were subsequently optimized with Density Functional Theory (DFT) in vacuum within the Gaussian 16 software[1]. The structure optimization, frequency analysis, energy level of frontier molecular orbital and electron reorganization energy were obtained at the Becke three-parameter Lee-Yang-Parr (B3LYP) [2] hybrid functional with the 6-31G(d) [3] basis set. The electronic coupling between dimer can be obtained by using Prof. Shuai's code based on the Equation below:

$$V = \frac{H_{12} - \frac{1}{2}(H_{11} + H_{22})S_{12}}{1 - S_{12}^2}$$

Here, H_{12}=$\langle\psi_1|H|\psi_2\rangle$, S_{12}=$\langle\psi_1|\psi_2\rangle$, H_{11}=$\langle\psi_1|H|\psi_1\rangle$, H_{22}=$\langle\psi_2|H|\psi_2\rangle$. H is the Kohn-Sham Hamiltonian of the dimer, $\psi_{1/2}$ means the LUMO of the monomer in the dimer for electron transport, S_{12} is the overlap integral. We obtained the transfer integrals at DFT/PW91PW91/6-31G(d) level. Besides, the Mercury software was employed to obtain the total packing energy in details.

Photoluminescence (PL).

The PL measurements were conducted by using FLS1000 equipment.

Temperature-dependent PL Spectra and Evaluation of Exciton Binding Energy (E_b)[4].

Temperature-dependent PL spectra varied from 150 to 300 K were measured by FLS1000 visible photomultiplier (PMT-900 nm) and infrared fluorescence spectrometer (PMT-1400 nm), with excitation at 765 nm for NFAs provided by 450W ozone-free continuous xenon lamp. The detection wavelength for CS1, CS2 and CS3 was 930 nm. The thin film samples were prepared by spin coating of solutions on the surface of SiO_2. The E_b values were obtained by fitting the temperature-varying PL intensities, I(T), with the Arrhenius equation:

$$I(\mathrm{T}) = \frac{I_0}{1 + \mathrm{A}e^{-\frac{E_b}{k_b \mathrm{T}}}}$$

Where I_0 is the PL intensity at the lowest temperature; T is the temperature; A is a constant; k_B is the Boltzmann constant.

Atomic Force Microscopy-Infrared Spectroscopy (AFM-IR).

The atomic force microscopy-infrared spectroscopy (AFM-IR) measurements were performed on Bruker NanoIR3 by using in tapping mode. AFM-IR images of the corresponding blend films (measured at a wavenumber of 2216 cm^{-1}, which is a characteristic absorption peak of SMAs, compared with PM6.

Space-Charge-Limited Current (SCLC) Measurement.

The SCLC method was used to measure the hole and electron mobilities, by using a diode configuration of ITO/PEDOT:PSS/active layer/MoO_3/Al for hole and ITO/ZnO/active layer/PNDIT-F3N/Al for electron. The dark current density curves were recorded with a bias voltage in the range of 0~8 V. The mobilities were estimated by taking current-voltage curves and fitting the results based on the equation listed

below:

$$J = \frac{9\varepsilon_0\varepsilon_\gamma\mu V^2}{8L^3}$$

where J is the current density, ε_0 is the vacuum permittivity, ε_r is the relative dielectric constant, μ is the mobility, and L is the film thickness. V (V_{app}–V_{bi}) is the internal voltage in the device, where V_{app} is the applied voltage to the device and V_{bi} is the built-in voltage due to the relative work function difference between the two electrodes.

Grazing Incidence Wide Angle X-ray Scattering (GIWAXS).

The GIWAXS samples were prepared on Si/PEDOT:PSS substrates by use of the same preparation conditions with devices and were carried out at XEUSS SAXS/WAXS equipment.

Energy Loss Analysis of OSCs.

The total E_{loss} was partitioned into three parts, as described below.

$$E_{loss} = (E_g - qV_{OC}^{SQ}) + (qV_{OC}^{SQ} - qV_{OC}^{rad}) + (qV_{OC}^{rad} - qV_{OC}) = \Delta E_1 + \Delta E_2 + \Delta E_3 \quad \text{(S8)}$$

The band gaps (E_g) of blended films, determined by the absorption and photoluminescence spectra of neat film. The V_{OC}^{SQ} is the maximum voltage based on the Shockley–Queisser (SQ) limit:

$$V_{oc}^{SQ} = \frac{kT}{q}\ln\left(\frac{J_{sc}^{SQ}}{J_0^{SQ}} + 1\right) \cong \frac{kT}{q}\ln\left(\frac{q\cdot\int_{E_g}^{+\infty}\phi_{AM1.5G}(E)\mathrm{d}E}{q\cdot\int_{E_g}^{+\infty}\phi_{BB}(E)\mathrm{d}E}\right)$$

The V_{OC}^{rad} is calculated from the EQE spectrum using the detailed balance theory:

$$V_{oc}^{rad} = \frac{kT}{q}\ln\left(\frac{J_{sc}}{J_0^{rad}} + 1\right) \cong \frac{kT}{q}\ln\left(\frac{q\cdot\int_{0}^{+\infty}\mathrm{EQE}(E)\phi_{AM1.5G}(E)\mathrm{d}E}{q\cdot\int_{0}^{+\infty}\mathrm{EQE}(E)\phi_{BB}(E)\mathrm{d}E}\right)$$

where q is the elementary charge and ϕ_{BB} is the black body spectrum at 300 K.

ΔE_3 is confirmed by directly measuring the external quantum efficiency of

electroluminescence (EQE_{EL}) of the solar cell through the equation below:

$$\Delta E_3 = kTln\left(\frac{1}{EQE_{EL}}\right)$$

Electroluminescence External Quantum Efficiency (EQE_{EL}).

For the EQE_{EL} measurements, a digital source meter (Keithley 2400) was employed to inject electric current into the solar cells, and the emitted photons were collected by a Si diode (Hamamatsu s1337-1010BQ) and indicated by a picometer (Keithley 6482). The injection current to the OSCs was kept at 1 mA by the direct current meter (PWS2326 Tectronix).

Contact angles Measurement.

The contact angles of two different solvents (water and glycerol) on the neat films (donor/acceptor) were measured on a JC2000D1 drop shape analyzer (POWEREACH®). The miscibility of two components in the blend can be estimated from the solubility parameters (δ) of each material, which can be calculated with equation: $\delta = K\sqrt{\gamma}$, where γ is the surface energy of the material, and K is the proportionality constant ($K = 116 \times 10^3$ $m^{1/2}$).

Single-crystal Growth.

Single crystal of CH-Th and CH-Ph were grown by the liquid diffusion method at room temperature. In detail, 1.5 mL of methanol was transferred to 0.10 mL of concentrated chloroform solution (1.5 mg/ml for CH-Th and 2 mg/ml for CH-Ph) of SMAs slowly, and the needle-shape dark purple crystals were formed on the inner glass tube after about 10 days. The X-ray diffraction signals of single crystal were collected on Rigaku XtalAB PRO MM007 DW. The crystal was kept at 193.0 K during data collection.

Device Fabrication.

The conventional devices based on PM6:CH-Th, PM6:CH-Ph and PM6:CH6F:CH-Th were fabricated with the architecture of ITO/ PEDOT: PSS /PM6:SMAs/PNDIT-

F3N/Ag. In detail, ITO coated glass substrates were cleaned in turn with detergent water, deionized water, acetone and isopropyl alcohol in an ultrasonic bath sequentially for 15 mins and dried by nitrogen purge. Before use, the cleaned ITO substrates were treated with UV exposure for 15 mins in a UV-ozone chamber (Jelight Company). Then a thin layer of poly (3,4-ethylene dioxythiophene): poly (styrene sulfonate) (PEDOT: PSS, Baytron PVP Al 4083) was first spin-coated on the ITO substrates with 3000 rpm for 20 s. Subsequently, the PEDOT: PSS films were baked at 150 ℃ for 20 mins under ambient conditions and transferred to a glove box quickly. Then the PM6:SMAs (D:A ratio= 1:1.2) were fully dissolved in chloroform (CF) with 0.5% 1-chloronaphthalene (CN) as an additive.at a total concentration of 13.2 mg mL^{-1}, and were spin-casted at 2000 rpm for 30 s onto the PEDOT: PSS layer. After spin-coating, the blend films were annealed at 90°C for 5 mins. The best active layer thickness is about 100 nm. PNDIT-F3N (dissolved in methanol with 0.5% v/v glacial acetic acid at the concentration of 1.0 mg mL^{-1}) layer was spin-coated on the top of the active layers at 3000 rpm for 20 s. Finally, 150 nm Ag was deposited under 2×10^{-6} Pa. The active area of the device was 4 mm^2. The area of the mask was about 3.24 mm^2 in our laboratory. The device illuminated area during testing was 7×7 cm^2. The device and mask areas were determined using an optical profilometer (PSM-1000).

Operation Stability Measurement. The operation stability of devices were measured under continuous light, which was generated by the LED system (MT-PV-64, TIANJIN METO) at 25 ± 2 °C in N_2 atmosphere without encapsulation. The LED spectrum is shown in Figure S10. The stabilized PCE was periodically measured with 1 sun illumination at 16 independent channels with MPP. The JV values were recorded using the multimeter (Mato-30) and software.

Thermal Stability Measurement. The thermal stability of devices were measured in N_2 atmosphere without encapsulation and carried out on a hot plate (WH200D-1K, WIGGENS, Germany) with a continuous thermal stress of 65 °C in dark conditions.

2. Synthesis

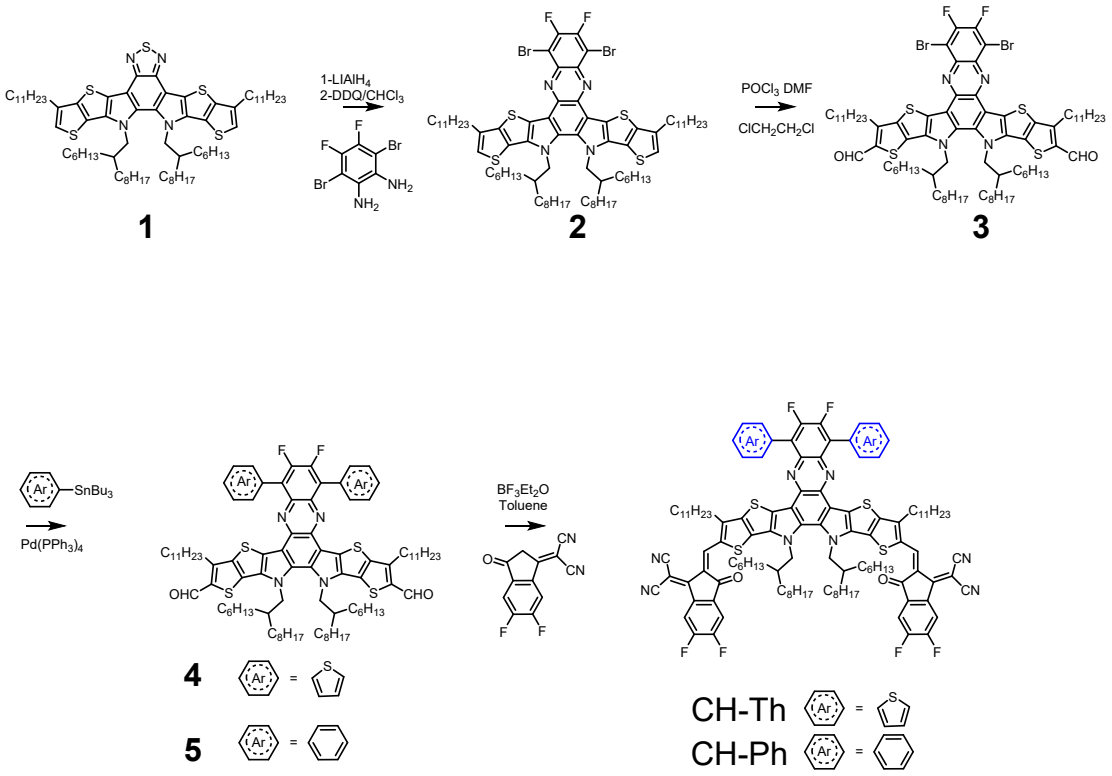

Scheme S1 The overall synthetic route to CH-Th and CH-Ph.

Synthesis of compound **2**.

20 ml $LiAlH_4$ (2.5M solution in tetrahydrofuran 50 mmol ,100 eq.) was added to a solution of compound **1** (600 mg, 0.50 mmol, 1.0 eq.) in tetrahydrofuran (THF, 60 mL) under the protection of argon at room temperature. The resulting mixture was stirred and heated to reflux for 12 h. After cooling to room temperature, the reaction mixture was dropped into ice cooled 150ml 1M HCl solution. The mixture was extracted with dichloromethane and the organic layer was dried with anhydrous Na_2SO_4. After removal of solvent, the crude product was dissolved in chloroform (45 mL), then 3-dichloro-5,6-dicyano-1,4-benzoquinone (DDQ, 113.5 mg, 0.50 mmol, 1.0 eq.) was added into the solution. The reaction was stirred at room temperature for 10 minutes. After that, 3,6-dibromo-4,5-difluorobenzene-1,2-diamine (755 mg, 2.5 mmol, 5 eq.) was added to the solution. The reaction was stirred for 6 hours at room temperature. After completion of the reaction, the solvent was removed by rotary evaporation to give the crude product, which was further purified by column chromatography on silica gel

with petroleum ether as eluent to afford **2** as a dark brown solid (201 mg, 28%). ^{1}H NMR (400 MHz, Chloroform-d) δ 7.04 (s, 2H), 4.68 (d, J = 7.9 Hz, 4H), 2.88 (t, J = 7.7 Hz, 4H), 2.24 – 2.13 (m, 2H), 1.90 (p, J = 7.6 Hz, 4H), 1.58 – 0.61 (m, 98H); ^{13}C NMR (101 MHz, Chloroform-d) δ 150.86, 148.51, 143.75, 138.21, 137.31, 137.06, 135.44, 123.62, 123.39, 119.26, 116.40, 109.01, 55.29, 38.78, 31.98, 31.82, 31.66, 30.52, 30.41, 29.78, 29.76, 29.74, 29.72, 29.67, 29.57, 29.53, 29.51, 29.47, 29.43, 29.40, 29.17, 28.88, 25.59, 22.74, 22.62, 22.51, 14.16, 14.11, 13.99; 1; MS (m/z, MALDI) Calcd for $C_{78}H_{114}Br_2F_2N_4S_4$ $[M+H]^+$1433.6341, found 1433.6325.

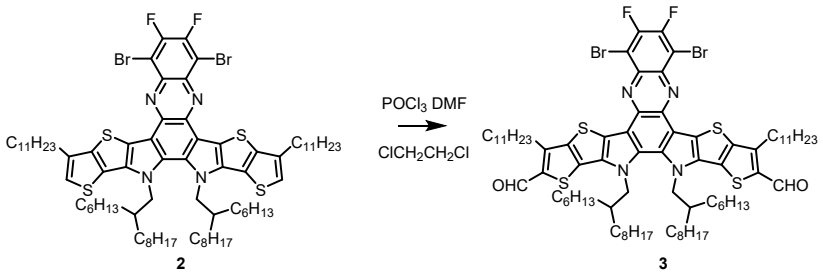

Synthesis of compound **3**.

Under the protection of argon, phosphorus oxychloride (0.6 mL) was added to a solution of compound **2** (200 mg) and N, N-Dimethylformamide (DMF, 3 mL) in 1, 2-dichloroethane ($ClCH_2CH_2Cl$, 50 mL). The resulting mixture was stirred and heated to reflux for 12 h, then cooled to 0 ℃. The resulting mixture was slowly added to a saturated solution of sodium acetate (40 mL), then stirred at room temperature for 2 h. The resulting mixture was extracted with dichloromethane and the organic layer was dried over anhydrous Na_2SO_4 for 0.5 h. After removal of solvent, the crude product was then purified by column chromatography on silica gel with petroleum ether/dichloromethane (v/v=5:2) as eluent to afford compound **3** as a brown solid (201 mg, 97%). ^{1}H NMR (400 MHz, Chloroform-d) δ 10.18 (s, 2H), 4.73 (d, J = 8.0 Hz, 4H), 3.28 (t, J = 7.6 Hz, 4H), 2.24 – 2.12 (m, 2H), 2.08 – 1.92 (m, 4H), 1.80 – 0.43 (m, 98H); ^{13}C NMR (101 MHz, $CDCl_3$) δ 181.85, 151.58, 151.37, 149.01, 147.01, 144.69, 138.22, 137.18, 137.04, 135.99, 133.24, 129.47, 128.27, 117.16, 109.11, 55.53, 42.41, 39.01, 38.78, 35.46, 34.77, 34.17, 32.75, 31.97, 31.94, 31.93, 31.79, 31.63, 31.59, 30.61, 30.50, 30.39, 29.74, 29.71, 29.66, 29.58, 29.55, 29.53, 29.44, 29.42, 29.39, 29.36,

29.33, 29.17, 29.07, 28.11, 27.99, 26.95, 26.75, 26.47, 26.36, 25.55, 23.00, 22.93, 22.73, 22.72, 22.68, 22.60, 22.50, 20.20, 19.19, 14.43, 14.18, 14.13, 14.12, 14.08, 13.96, 11.42; MS (m/z, MALDI) Calcd for $C_{80}H_{114}Br_2F_2N_4O_2S_4$ $[M+H]^+$1489.6239, found 1489.6220.

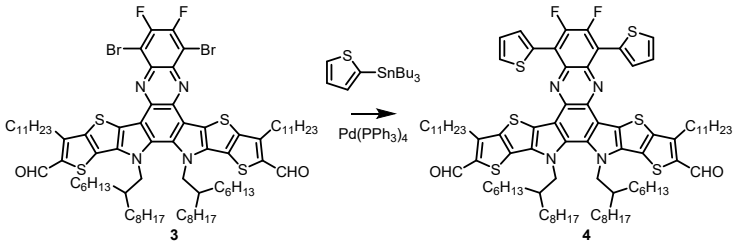

Synthesis of compound **4**.

Compound **3** (200 mg, 0.13 mmol, 1 eq.) and tributyl(thiophen-2-yl)stannane (200 mg, 0.54 mmol, 4 eq.) were dissolved in 30ml dried toluene. Then $Pd(PPh_3)_4$ (62 mg, 0.05 mmol, 0.4eq.) was added to the reaction mixture under the protection of argon. The mixture was refluxed for 16 hours. After cooling to room temperature 20 ml of saturated KF aqueous solution was added to the reaction mixture and the mixture was stirred at room temperature for 30 minutes. The resulting mixture was extracted with dichloromethane and the organic layer was dried over anhydrous Na_2SO_4 for 0.5 h. After removal of solvent, the crude product was then purified by column chromatography on silica gel with petroleum ether/dichloromethane (v/v=2:1) as eluent to afford compound **4** as a red solid (185 mg, 92%). ^{1}H NMR (400 MHz, Chloroform-d) δ 10.17 (s, 2H), 8.17 (d, J = 3.7 Hz, 2H), 7.77 (d, J = 5.1 Hz, 2H), 7.43 (t, J = 4.5 Hz, 2H), 4.69 (d, J = 7.8 Hz, 4H), 3.24 (t, J = 7.8 Hz, 4H), 2.05 (dt, J = 42.9, 7.0 Hz, 6H), 1.74 – 0.50 (m, 98H); ^{13}C NMR (101 MHz, $CDCl_3$) δ 181.78, 146.78, 144.14, 137.09, 137.01, 133.42, 131.57, 129.42, 128.25, 128.18, 126.80, 117.80, 55.35, 38.96, 31.96, 31.80, 31.62, 30.41, 30.35, 30.27, 29.89, 29.75, 29.70, 29.55, 29.45, 29.41, 29.37, 29.20, 28.25, 25.48, 22.73, 22.60, 22.54, 14.15, 14.10, 14.01; MS (m/z, MALDI) Calcd for $C_{88}H_{120}F_2N_4O_2S_6$ $[M+H]^+$1495.7804, found 1495.7721.

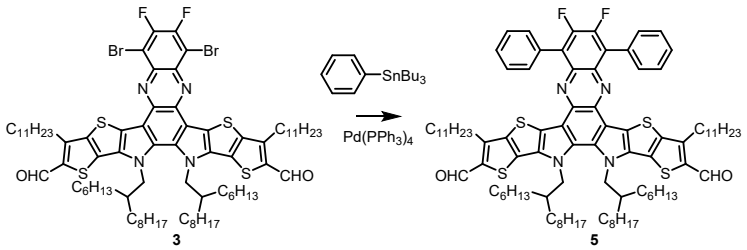

Synthesis of compound **5**.

Compound **3** (200 mg, 0.13 mmol, 1 eq.) and tributyl(phenyl)stannane (198 mg, 0.54 mmol, 4 eq.) were dissolved in 30ml dried toluene. Then $Pd(PPh_3)_4$ (62 mg, 0.05 mmol, 0.4eq.) was added to the reaction mixture under the protection of argon. The mixture was refluxed for 16 hours. After cooling to room temperature 20 ml of saturated KF aqueous solution was added to the reaction mixture and the mixture was stirred at room temperature for 30 minutes. The resulting mixture was extracted with dichloromethane and the organic layer was dried over anhydrous Na_2SO_4 for 0.5 h. After removal of solvent under reduced pressure, the crude product was then purified by column chromatography on silica gel with petroleum ether/dichloromethane (v/v=2:1) as eluent to afford compound **4** as a red solid (157 mg, 79%). ^{1}H NMR (400 MHz, Chloroform-d) δ 10.16 (s, 2H), 7.98 (d, J = 7.5 Hz, 4H), 7.74 (t, J = 7.6 Hz, 4H), 7.65 (d, J = 7.4 Hz, 2H), 4.65 (d, J = 7.8 Hz, 4H), 3.21 (t, J = 7.8 Hz, 4H), 2.13 – 2.07 (m, 2H), 1.96 (h, J = 7.7 Hz, 4H), 1.66 – 0.64 (m, 98H); ^{13}C NMR (101 MHz, $CDCl_3$) δ 181.72, 146.76, 144.41, 137.50, 136.87, 136.78, 136.68, 132.68, 132.10, 131.44, 131.24, 129.48, 128.22, 128.19, 128.15, 125.57, 117.83, 55.34, 38.91, 34.71, 31.96, 31.93, 31.77, 31.63, 31.57, 30.40, 30.35, 30.22, 30.02, 29.75, 29.71, 29.57, 29.46, 29.43, 29.41, 29.32, 29.17, 28.30, 26.95, 25.52, 25.49, 25.32, 22.73, 22.70, 22.58, 22.51, 14.15, 14.09, 13.98; MS (m/z, MALDI) Calcd for $C_{92}H_{124}F_2N_4O_2S_4$ $[M+H]^+$1483.8675, found 1483.8595.

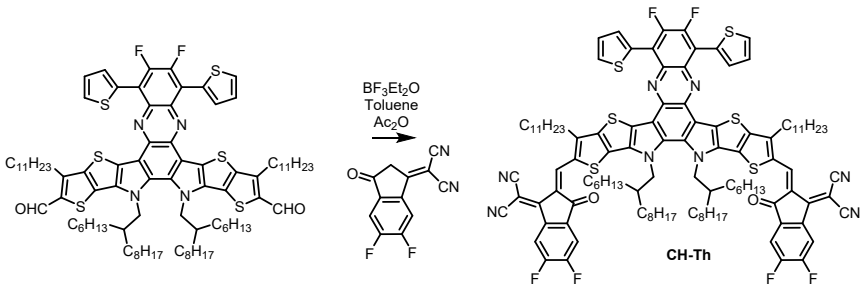

Synthesis of **CH-Th**.

Compound **4** (100 mg 0.067 mmol 1 eq.) and 2-(5,6-difluoro-3-oxo-2,3-dihydro-1H-inden-1-ylidene) malononitrile (46 mg 0.20 mmol 3eq.) were dissolved in 15 ml dried toluene, then 0.2ml acetic anhydride and 0.2 ml boron trifluoride etherate were added to the reaction mixture successively. The reaction was stirred at room temperature under ambient atmosphere for 30 minutes. The reaction mixture was precipitated in 100 mL methanol. The precipitate was purified by column chromatography on silica gel with petroleum ether/ chloroform (v/v=1/1) as eluent to give black compound CH-Th (107 mg 83%) ^{1}H NMR (400 MHz, Chloroform-d) δ 9.18 (s, 2H), 8.57 (dd, J = 9.9, 6.4 Hz, 2H), 8.13 (d, J = 3.6 Hz, 2H), 7.79 (dd, J = 5.1, 1.2 Hz, 2H), 7.70 (t, J = 7.5 Hz, 2H), 7.45 (dd, J = 5.2, 3.6 Hz, 2H), 4.82 (d, J = 7.8 Hz, 4H), 3.26 (t, J = 7.9 Hz, 4H), 2.26 – 2.12 (m, 2H), 1.94 (p, J = 7.6 Hz, 4H), 1.57 – 0.63 (m, 98H); ^{13}C NMR (101 MHz, $CDCl_3$) δ 186.10, 158.88, 155.61, 155.51, 153.88, 153.30, 153.00, 146.11, 137.87, 136.82, 135.86, 135.26, 134.52, 133.36, 131.75, 131.59, 130.13, 128.40, 126.90, 119.82, 118.92, 115.03, 114.86, 114.62, 112.48, 112.28, 68.55, 55.72, 39.22, 31.93, 31.85, 31.64, 31.12, 30.60, 30.53, 30.07, 29.86, 29.82, 29.73, 29.69, 29.55, 29.51, 29.41, 29.39, 29.22, 25.60, 22.69, 22.59, 22.52, 14.11, 14.05; MS (m/z, MALDI) Calcd for $C_{112}H_{124}F_6N_8O_2S_6$ $[M]^+$1919.8112, found 1919.8109.

Synthesis of **CH-Ph**.

Compound **5** (100 mg 0.067 mmol 1 eq.) and 2-(5,6-difluoro-3-oxo-2,3-dihydro-1H-inden-1-ylidene) malononitrile (46 mg 0.20 mmol 3eq.) were dissolved in 15 ml dried toluene, then 0.2ml acetic anhydride and 0.2 ml boron trifluoride etherate were added to the reaction mixture successively. The reaction was stirred at room temperature under ambient atmosphere for 30 minutes. The reaction mixture was precipitated in 100 mL methanol. The precipitate was purified by column chromatography on silica gel with petroleum ether/ chloroform (v/v=1/1) as eluent to give black compound CH-Th (107 mg 83%) ^{1}H NMR (400 MHz, Chloroform-d) δ 9.18 (s, 2H), 8.63 – 8.55 (m, 2H), 7.94 (d, J = 7.6 Hz, 4H), 7.78 – 7.62 (m, 8H), 4.76 (d, J = 7.9 Hz, 4H), 3.23 (t, J = 8.1 Hz, 4H), 2.20 – 2.07 (m, 2H), 1.90 (d, J = 7.9 Hz, 4H), 1.63 – 0.82 (m, 86H), 0.75 (t, J =

7.2 Hz, 6H), 0.68 (t, J = 6.9 Hz, 6H). ^{13}C NMR (101 MHz, $CDCl_3$) δ 186.09, 158.67, 155.65, 153.86, 153.03, 150.77, 148.41, 146.55, 137.90, 137.68, 136.95, 136.62, 136.57, 136.02, 135.02, 134.48, 133.80, 132.00, 131.77, 131.01, 128.26, 125.77, 119.57, 119.11, 115.07, 114.98, 114.77, 114.63, 112.40, 112.21, 68.28, 55.78, 39.30, 34.71, 31.97, 31.89, 31.67, 31.63, 31.16, 30.64, 30.58, 30.29, 30.00, 29.89, 29.78, 29.75, 29.71, 29.64, 29.58, 29.54, 29.43, 29.27, 29.10, 26.95, 25.76, 25.32, 22.73, 22.70, 22.65, 22.63, 22.58, 14.15, 14.09. MS (m/z, MALDI) Calcd for $C_{116}H_{128}F_6N_8O_2S_4$ $[M]^+$1907.8981, found 1919.8968.

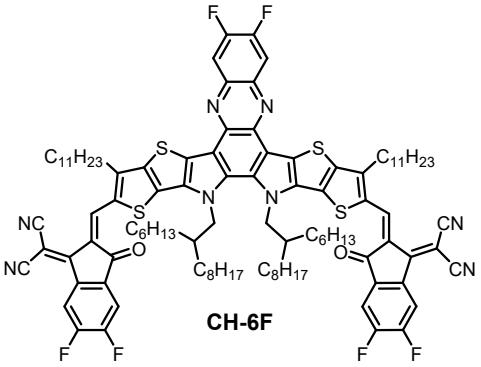

Figure S1 Chemical structure of CH6F.

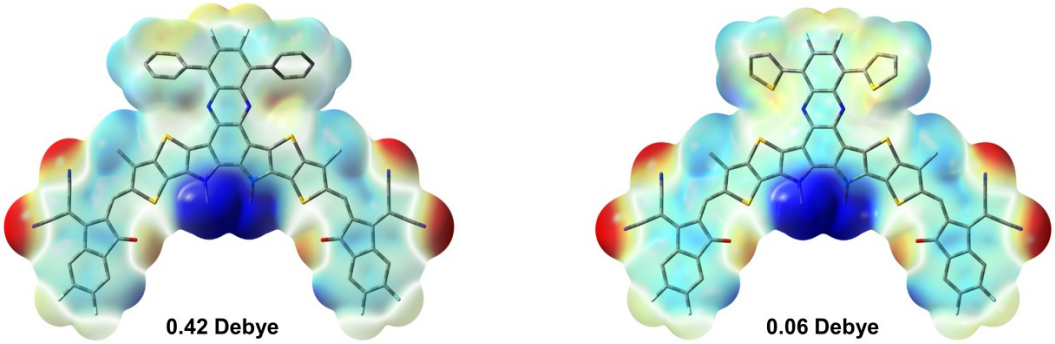

Figure S2 Electrostatic surface potential (ESP) maps with dipole moment values of CH-Ph and CH-Th.

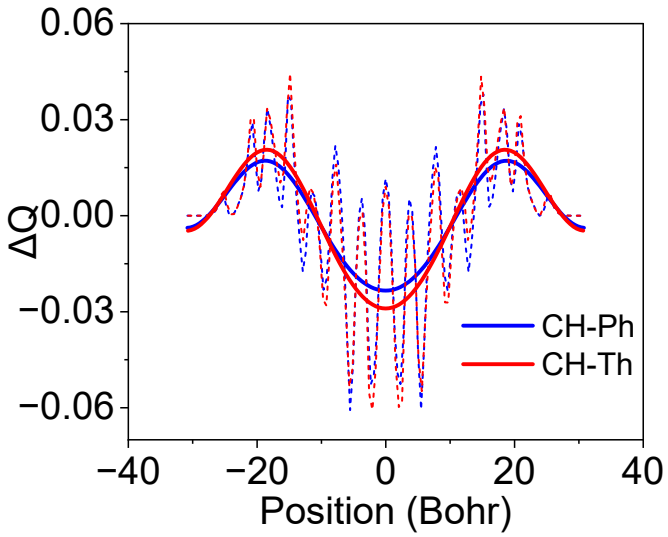

Figure S3 Charge density difference (ΔQ) of frontier molecular orbitals.

Table S1 The detailed parameters of theoretical isotropic polarizability and dipole moment of SMAs.

	Theoretical isotropic polarizability $Bohr^3$
CH-Th	1469.46
CH-Ph	1464.47

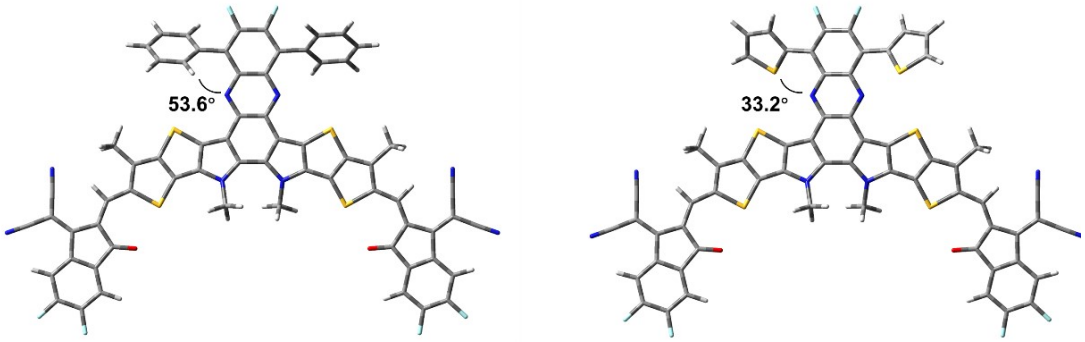

Figure S4 Optimized structures of CH-Ph and Ch-Th.

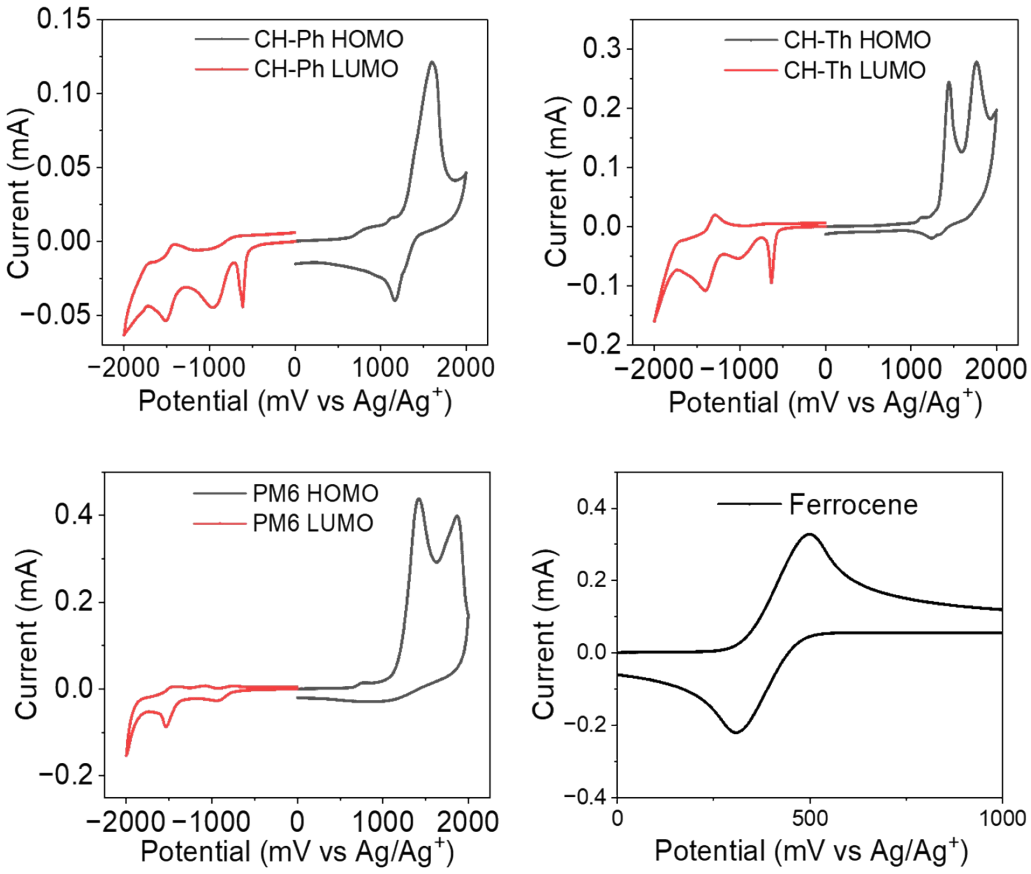

Figure S5 Cyclic voltammograms of CH-Ph, CH-Th and PM6 films. Red line: reduction cycle, black line: oxidation cycle.

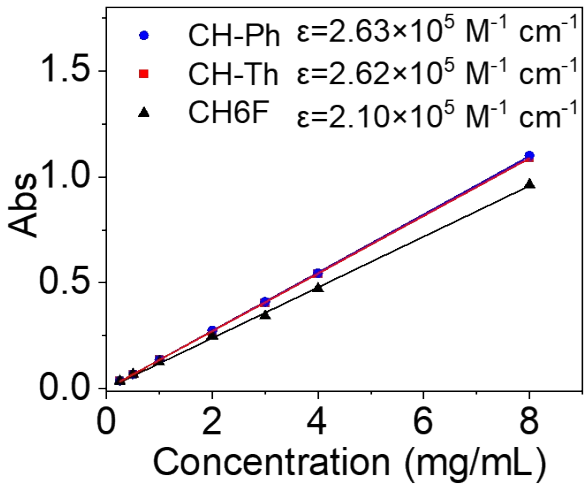

Figure S6 The molar extinction coefficients of CH6F, CH-Th and CH-Ph in dilute chloroform solutions.

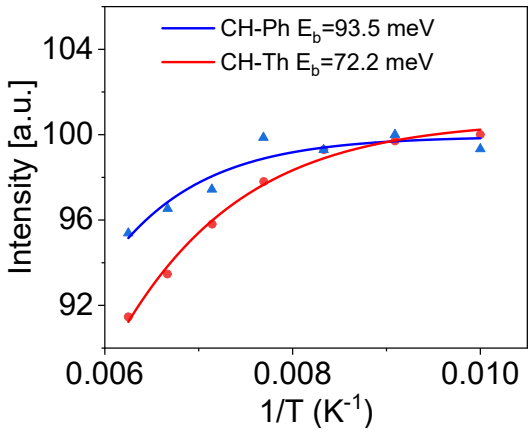

Figure S7 Exciton binding energies estimated from temperature-depend PL.

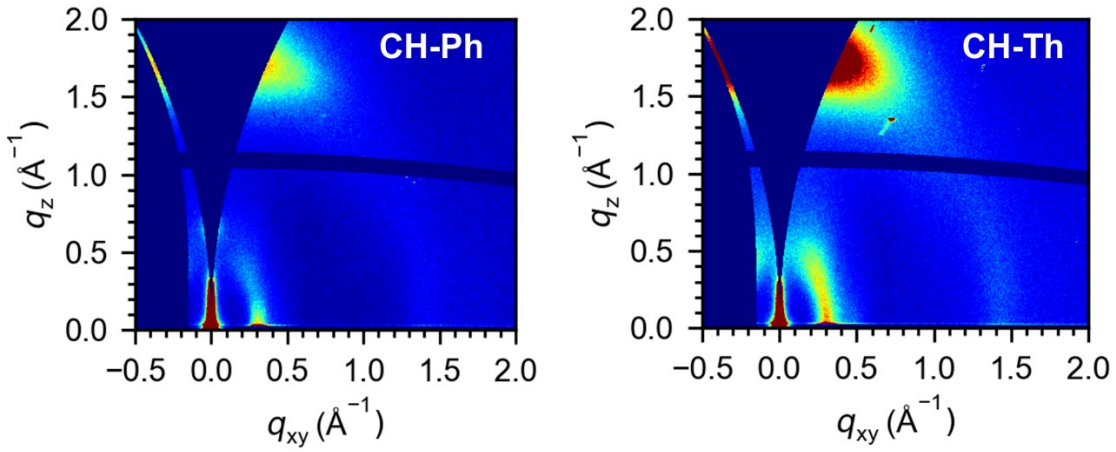

Figure S8 2D-GIWAXS of neat films.

Table S2 The detailed parameters of corresponding 2D GIWAXS of neat films in IP and OOP direction.

IP(100)	q(Å^{-1})[a]	d(Å)	CCL(Å)[b]	FWHM
CH-Th	0.31	20.27	75.62	0.075
CH-Ph	0.3025	20.77	71.81	0.079
OOP(010)	q(Å^{-1})	d(Å)[a]	CCL(Å)[b]	FWHM
CH-Th	1.72	3.65	23.77	0.24
CH-Ph	1.70	3.69	16.30	0.35

[a]Calculated from the equation: d-spacing=$2\pi/q$. [b]Obtained from the Scherrer equation: CCL= 2πK/FWHM, where FWHM is the full-width at half-maximum and K is a shape factor (K= 0.9 here).

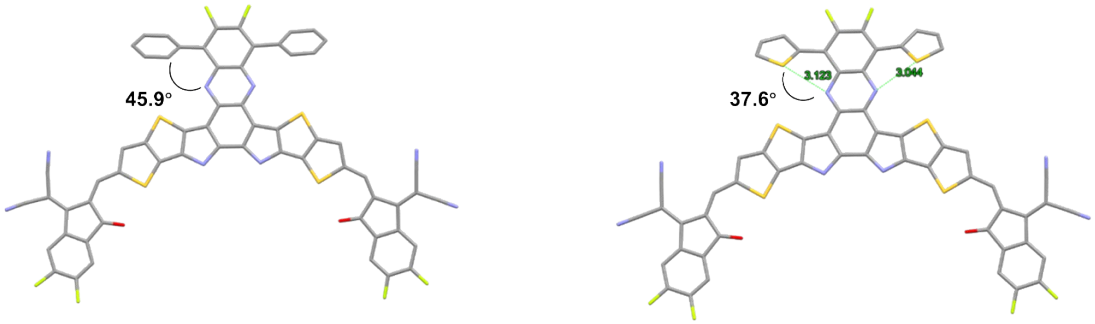

Figure S9 Monomolecular single crystal structure of CH-Ph and CH-Th on top view. The alkyl chains and hydrogen atoms were omitted for clarity.

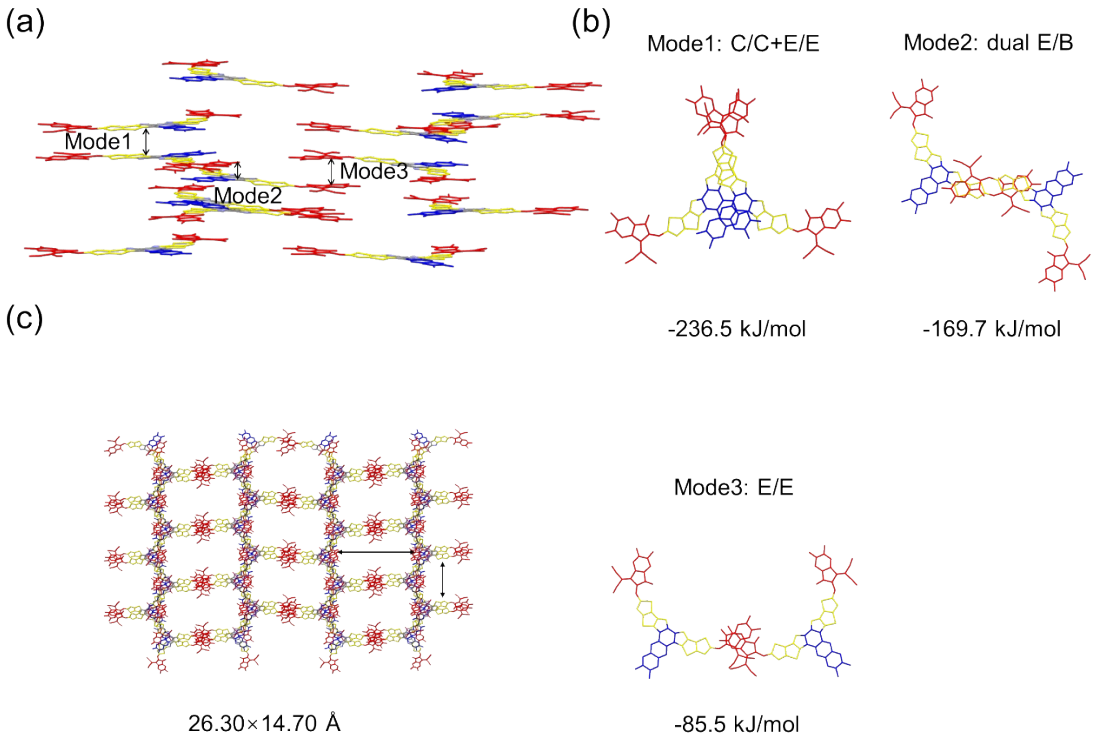

Figure S10 (a) Intermolecular potentials of interlayer including all main packing modes of CH6F. (b) Single crystal topological packing structures of CH6F on the top view. (c) Detailed packing modes of CH6F.[5]

Table S3 Crystal data and structure refinement for CH-Th and CH-Ph.

Compound	CH-Th	CH-Ph
Empirical formula	$C_{112}H_{124}F_6N_8O_2S_6$	$C_{112}H_{124}F_6N_8O_2S_6$
Formula weight	1920.54	1908.50
Temperature/K	193	193
Crystal system	monoclinic	triclinic
Space group	C2/c	P-1
a/Å	32.558(9)	22.346(2)
b/Å	33.376(9)	23.028(3)
c/Å	22.578(6)	23.090(3)
α/°	90	90.870(6)
β/°	103.160(12)	99.822(5)
γ/°	90	99.874(5)
Volume/Å^3	23891(11)	11522(2)
Z	8	4
ρ_{calc}g/cm^3	1.068	1.100
μ/mm^{-1}	0.985	0.800
F(000)	8144.0	4056.0
Crystal size/mm^3	0.12 × 0.1 × 0.08	0.12 × 0.1 × 0.09
Radiation	GaKα (λ=1.34139 Å)	GaKα (λ = 1.34139 Å)
2Θ range for data collection/°	5.222 to 108.044	3.546 to 109.054
Index ranges	-37 ≤ h ≤ 38, -40 ≤ k ≤ 39, -27 ≤ l ≤ 26	-26 ≤ h ≤ 26, -27 ≤ k ≤ 27, -26 ≤ l ≤ 27
Reflections collected	88923	131444
Independent reflections	21263 [R_{int} = 0.1996, R_{sigma} = 0.1690]	42454 [R_{int} = 0.1326, R_{sigma} = 0.1623]
Goodness-of-fit on F^2	1.160	0.959

Final R indexes [I>=2σ (I)]	R_1 = 0.1650, wR_2 = 0.3684	R_1 = 0.1554, wR_2 = 0.3431
Final R indexes [all data]	R_1 = 0.3248, wR_2 = 0.4331	R_1 = 0.3041, wR_2 = 0.4141
Largest diff. peak/hole / e $Å^{-3}$	0.58/-0.60	0.48/-0.49

Table S4 Crystallographic and π-π interaction parameters of CH-Ph and CH-Th.

SMAs	Void sizes (shapes)	Packing modes	Intermolecular potentials (kJ/mol)	$d_{\pi-\pi}$ [Å]	$^{c}V_E$ [meV]	V_H [meV]	d_{S-N} [Å]
Ch-Ph	31.4× 14.4 Å (rectangle)	Mode 1 (dual E/C)	-460.3	3.55	2.74	9.19	-
		Mode 2 (dual E/B)	-256.7	3.30	25.74	60.12	
		Mode 3 (dual E/C)	-170.6	5.37	0.40	2.86	-
		Mode 4 (E/E)	-115.8	4.56	2.73	2.46	
CH-Th	34.4× 8.3 Å (rectangle)	Mode 1 (dual E/C)	-448.7	3.46	3.47	2.61	3.04/3.12
		Mode 2 (C/C+E/E)	-246.7	3.46/3.26	9.36	12.28	
		Mode 3 (dual E/B)	-181.3	3.98	12.82	63.64	
		Mode 4 (E/E)	-96.4	2.58	1.84	0.35	

CH6F	26.3× 14.7 Å (rectangle)	Mode 1 (C/C+E/E)	-236.5	3.35/3.80 (3.57 in average)	60.5	42.5	-
		Mode 2 (dual E/B)	-169.7	3.38	16.0	38.8	
		Mode 3 (Dual E/E)	-85.5	3.47	22.7	4.9	

Table S5 Detailed photovoltaic parameters of the PM6:CH-Ph based devices under the illumination of AM 1.5 G, 100 mW cm^{-2}.

Active layer	V_{oc} [V]	J_{sc} [mA/cm^2]	FF [%]	PCE [%]
PM6:CH-Ph	0.907	24.47	77.60	17.22
	0.910	24.57	76.71	17.15
	0.908	24.45	77.67	17.24
	0.914	25.30	77.36	17.89
	0.912	25.34	76.99	17.79
	0.911	25.28	77.24	17.79
	0.910	25.28	77.04	17.72
	0.908	24.96	76.69	17.38
	0.909	25.25	76.88	17.65
	0.908	25.22	76.82	17.59
	0.915	25.30	75.86	17.56
	0.911	25.04	74.70	17.04
	0.909	25.22	74.80	17.15
	0.914	25.68	75.88	17.81
	0.910	24.57	76.71	17.15
	0.910±0.002	25.06±0.38	76.60±0.91	17.48±0.30

Table S6 Detailed photovoltaic parameters of the PM6:CH-Th based devices under the illumination of AM 1.5 G, 100 mW cm^{-2}.

Active layer	V_{oc} [V]	J_{sc} [mA/cm^2]	FF [%]	PCE [%]
PM6:CH-Th	0.933	26.47	75.62	18.68
	0.932	26.41	77.01	18.96
	0.930	26.29	76.06	18.60
	0.929	26.45	75.85	18.64
	0.928	26.72	75.44	18.71
	0.925	26.43	76.08	18.60
	0.927	26.56	75.90	18.69
	0.927	26.64	75.44	18.63
	0.928	26.56	75.51	18.61
	0.924	26.64	75.66	18.62
	0.922	26.71	75.72	18.65
	0.923	26.84	75.32	18.66
	0.929	26.49	75.92	18.68
	0.926	26.58	75.90	18.68
	0.927	26.45	76.17	18.68
	0.927±0.003	26.55±0.14	75.84±0.41	18.67±0.09

Table S7 Detailed photovoltaic parameters of the PM6:CH6F based devices under the illumination of AM 1.5 G, 100 mW cm^{-2}.

Active layer	V_{oc} [V]	J_{sc} [mA/cm^2]	FF [%]	PCE [%]
PM6:CH-6F	0.871	25.75	74.92	16.80
	0.872	25.10	76.10	16.65
	0.873	25.12	74.15	16.26
	0.877	25.18	74.06	16.35
	0.877	25.50	75.45	16.87
	0.875	25.43	75.08	16.71
	0.874	25.56	75.90	16.95
	0.872	25.64	74.51	16.66
	0.873	25.36	74.62	16,52
	0.874	25.31	75.02	16.59
	0.872	24.71	75.72	16.31
	0.872	24.54	75.06	16.06
	0.869	25.69	75.31	16.81
	0.875	24.99	75.12	16.42
	0.877	25.45	74.17	16.55
	0.873±0.002	25.29±0.35	75.01±0.62	16.57±0.26

Table S8 Information about surface energies of CH6F, CH-Ph, CH-Th and PM6 films calculated by water and glycerol contact angle.

Materials	γ_d (mN m^{-1})	γ_p (mN m^{-1})	γ (mN m^{-1})	χ^{D-A} (PM6)	χ (CH6F)
CH6F	1.1	24.1	25.2	0.19	-
CH-Ph	3.0	21.5	24.5	0.13	0.05
CH-Th	3.1	22.9	26.0	0.27	0.06
PM6	0.7	20.3	21.0	-	0.19

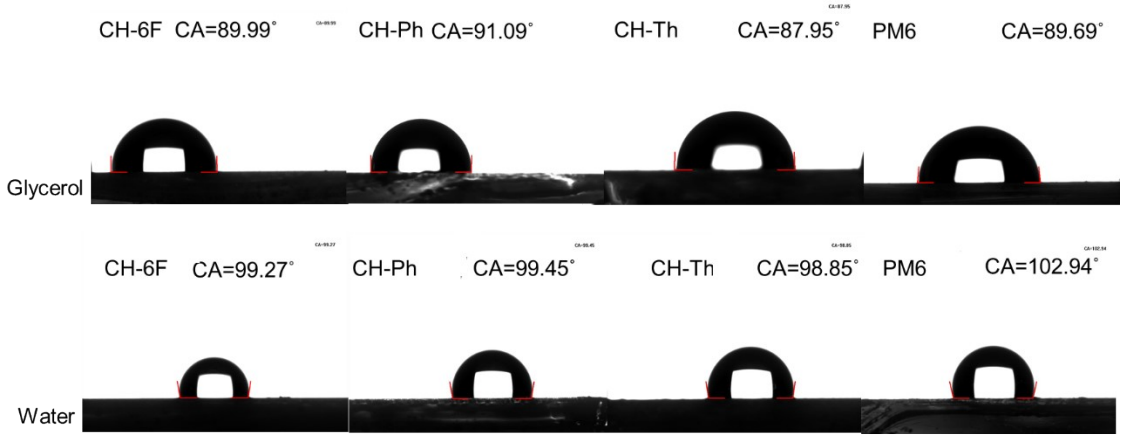

Figure S11 The images of water and glycerol drops on PM6, CH6F, CH-Ph and CH-Th films.

Table S9 Detailed photovoltaic parameters of the PM6:CH6F:CH-Th based devices under the illumination of AM 1.5 G, 100 mW cm^{-2}.

Active layer	V_{oc} [V]	J_{sc} [mA/cm^2]	FF [%]	PCE [%]
PM6:CH6F:CH-Th (1:1:0.2)	0.876	28.18	80.28	19.82
	0.873	28.10	80.43	19.73
	0.872	28.15	80.55	19.77
	0.871	28.11	80.39	19.68
	0.871	28.29	80.54	19.85
	0.876	28.24	80.62	19.94
	0.874	28.25	80.62	19.91
	0.874	28.09	80.68	19.81
	0.873	28.14	80.54	19.79
	0.874	28.19	80.56	19.85
	0.872	28.13	80.62	19.78
	0.872	28.10	80.89	19.82
	0.876	28.07	80.37	19.76
	0.874	27.91	80.78	19.70
	0.873	28.03	80.45	19.69
	0.873±0.002	28.13±0.09	80.55±0.16	19.79±0.08

Table S10 Detailed photovoltaic parameters of the PM6:CH-Ph based devices processed from **o-xylene** under the illumination of AM 1.5 G, 100 mW cm^{-2}.

Active layer	V_{oc} [V]	J_{sc} [mA/cm^2]	FF [%]	PCE [%]
PM6:CH-Ph (1:1.2)	0.897	23.22	80.25	16.71
	0.898	22.60	80.09	16.25
	0.897	22.42	79.96	16.08
	0.899	23.31	79.50	16.66
	0.897	23.25	79.57	16.58
	0.895	23.41	79.24	16.61
	0.894	23.18	79.75	16.53
	0.893	23.35	79.02	16.48
	0.894	23.32	79.39	16.56
	0.894	23.26	79.39	16.50
	0.891	23.26	79.16	16.41
	0.891	23.33	79.14	16.45
	0.892	23.11	79.84	16.46
	0.891	23.34	78.39	16.30
	0.891	23.07	79.76	16.40
	0.894±0.003	23.19±0.27	79.35±0.60	16.44±0.16

Table S11 Detailed photovoltaic parameters of the PM6:CH-Th based devices processed from o-xylene under the illumination of AM 1.5 G, 100 mW cm^{-2}.

Active layer	V_{oc} [V]	J_{sc} [mA/cm^2]	FF [%]	PCE [%]
PM6:CH-Th (1:1.2)	0.921	22.48	77.85	16.11
	0.918	22.39	77.97	16.04
	0.915	21.97	78.63	15.80
	0.913	21.85	77.85	15.54
	0.913	22.36	77.77	15.88
	0.912	22.26	78.32	15.90
	0.911	22.28	78.65	15.96
	0.910	21.70	79.03	15.60
	0.909	21.85	77.86	15.46
	0.918	22.28	78.00	15.95
	0.911	21.68	78.39	15.48
	0.910	21.60	78.43	15.42
	0.910	21.50	78.77	15.41
	0.918	22.51	78.01	16.12
	0.915	22.57	78.66	16.24
	0.913±0.004	22.02±0.34	78.27±0.41	15.73±0.25

Table S12 Detailed photovoltaic parameters of the PM6:CH6F:CH-Th based devices processed from o-xylene under the illumination of AM 1.5 G, 100 mW cm^{-2}.

Active layer	V_{oc} [V]	J_{sc} [mA/cm^2]	FF [%]	PCE [%]
PM6:CH6F:CH-Th (1:1:0.2)	0.883	23.56	79.36	16.52
	0.881	23.30	79.63	16.35
	0.875	23.56	79.69	16.43
	0.880	23.61	80.01	16.62
	0.875	23.52	79.00	16.26
	0.876	23.52	79.43	16.36
	0.875	23.66	78.89	16.34
	0.873	23.68	79.19	16.38
	0.872	23.49	79.44	16.27
	0.870	23.33	79.28	16.09
	0.868	23.44	79.23	16.13
	0.869	23.34	79.00	16.02
	0.871	23.47	79.14	16.18
	0.871	23.50	79.34	16.24
	0.871	23.64	78.73	16.20
	0.873±0.004	23.48±0.16	79.19±0.32	16.22±0.14

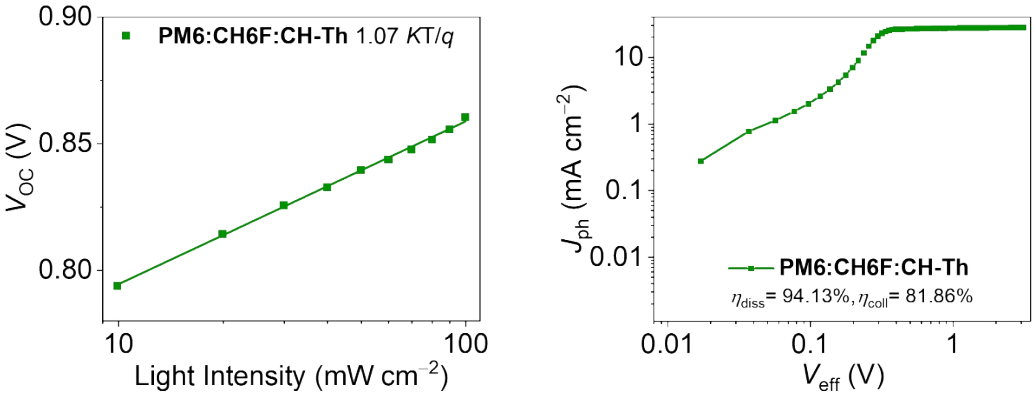

Figure S12 J_{ph} versus V_{eff} curves indicating P_{diss} and P_{coll}. P_{light} dependence of *V*oc for ternary devices.

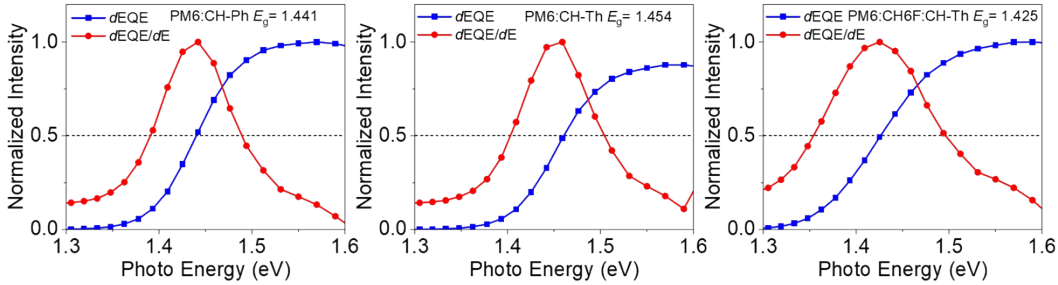

Figure S13 Details of optical E_g determination for PM6:CH-Ph, PM6:CH-Th and PM6:CH6F:CH-Th blend films.

Table S13 Detailed parameters for energy loss analysis of OSCs.

Active layer	V_{OC} (V)	E_g (eV)	V_{OC}^{SQ} (V)	ΔE_1 (eV)	V_{OC}^{rad} (V)	ΔE_2 (eV)	EQE_{EL} [10^{-2}]	ΔE_3 (eV)	E_{loss} (eV)
PM6:CH-Ph	0.914	1.441	1.174	0.267	1.099	0.075	0.045	0.185	0.527
PM6:CH-Th	0.932	1.454	1.186	0.268	1.106	0.080	0.056	0.174	0.522
PM6:CH6F:CH-Th	0.876	1.425	1.160	0.265	1.084	0.076	0.029	0.208	0.549

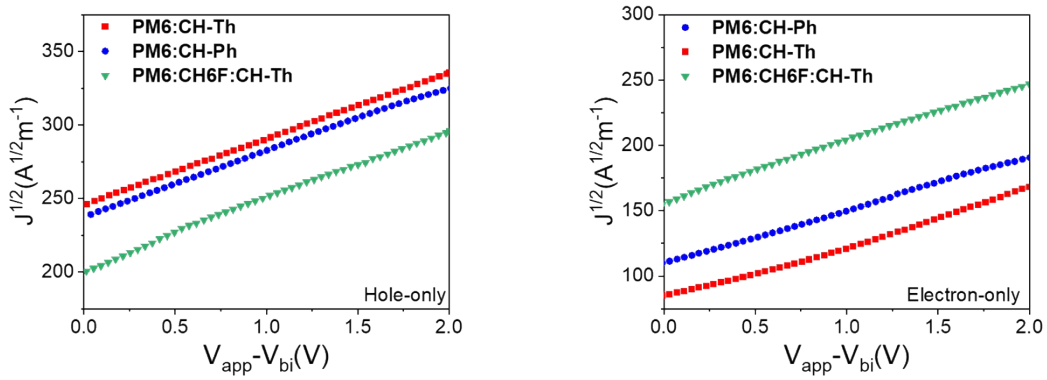

Figure S14 SCLC characteristics of hole-only and electron-only devices of blend films.

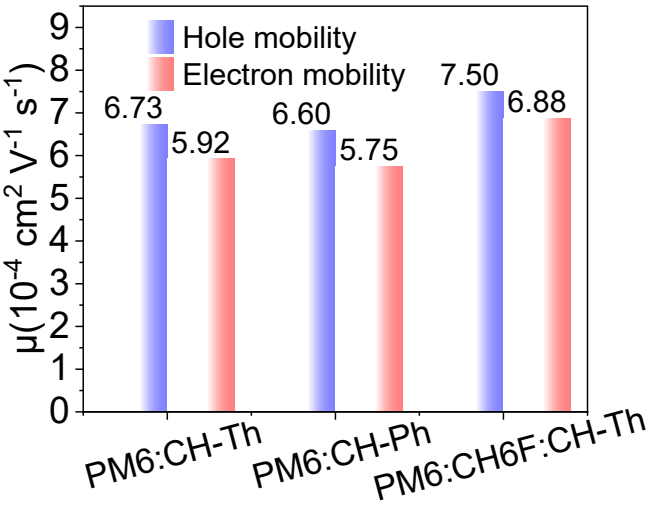

Figure S15 Charge mobility of blend films.

Table S14 The detailed parameters of hole and electron mobilities of blend films.

Materials	**Hole mobility (μ_h)** 10^{-4} **cm^2 V^{-1}s^{-1}**	**Electron mobility (μ_e)** 10^{-4} **cm^2 V^{-1}s^{-1}**	μ_h/μ_e
PM6:CH-Ph	6.60	5.75	1.15
PM6:CH-Th	6.73	3.17	2.12
PM8:CH6F:CH-Th	7.50	6.88	1.09

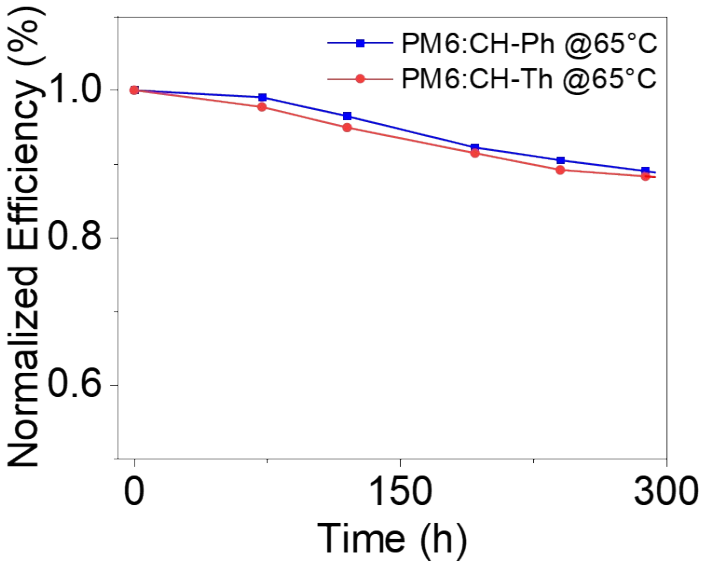

Figure S16 Thermal stability of devices

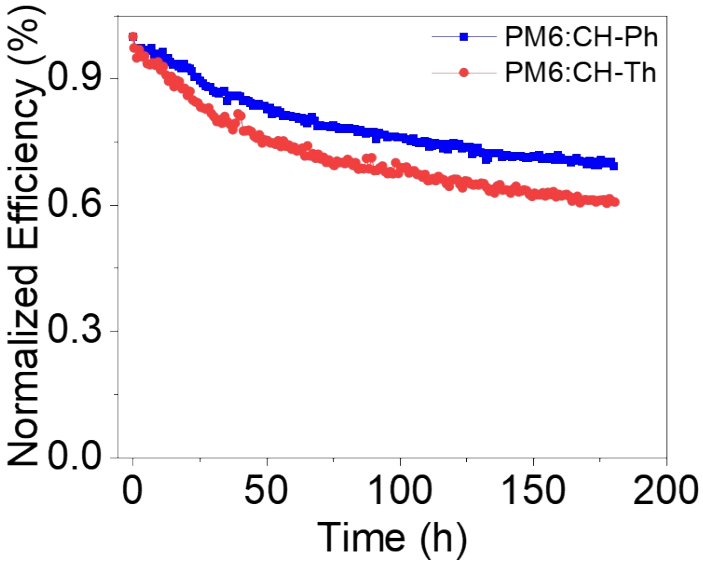

Figure S17 Light stability of devices

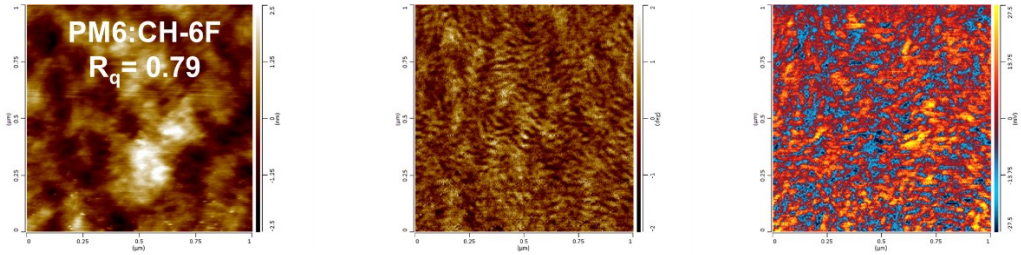

Figure S18 AFM height and phase images and AFM-IR image of PM6:CH6F blend films.

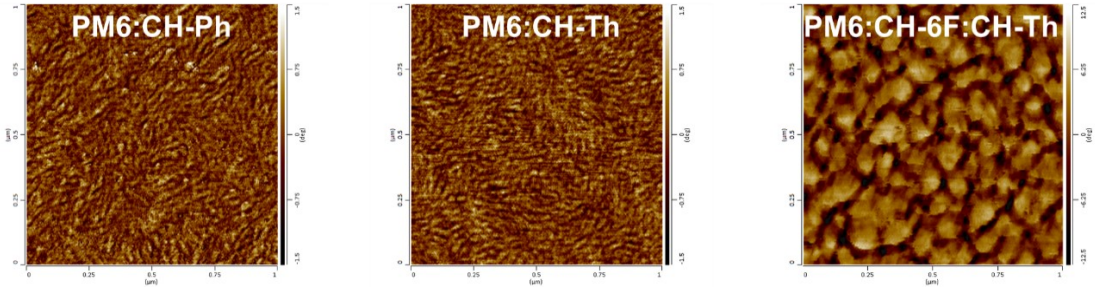

Figure S19 AFM phase images of PM6:CH-Ph, PM6:CH-Th and PM6:CH6F:CH-Th blend films.

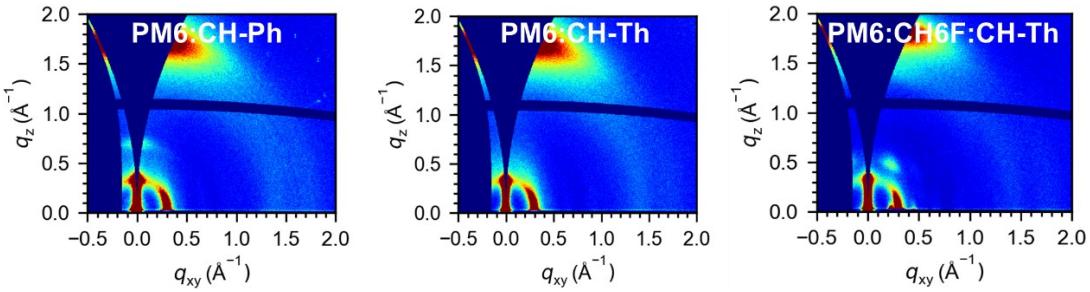

Figure S20 2D-GIWAXS of blend films.

Table S15 The detailed parameters of corresponding 2D GIWAXS of blend films in IP and OOP direction.

IP(100)	q(Å^{-1})	d(Å)[a]	CCL(Å)[b]	FWHM
PM6:CH-Ph	0.310	20.27	94.55	0.060
PM6:CH-Th	0.302	20.77	103.85	0.054
PM6:CH-Ph:CH-Th	0.300	20.94	190.85	0.030
PM6:CH-Ph	1.73	3.63	28.42	0.20
PM6:CH-Th	1.74	3.60	32.90	0.17
PM6:H-Ph:CH-Th	1.82	3.46	41.39	0.14

[a]Calculated from the equation: d-spacing=$2\pi/q$. [b]Obtained from the Scherrer equation: CCL= 2πK/FWHM, where FWHM is the full-width at half-maximum and K is a shape factor (K= 0.9 here).

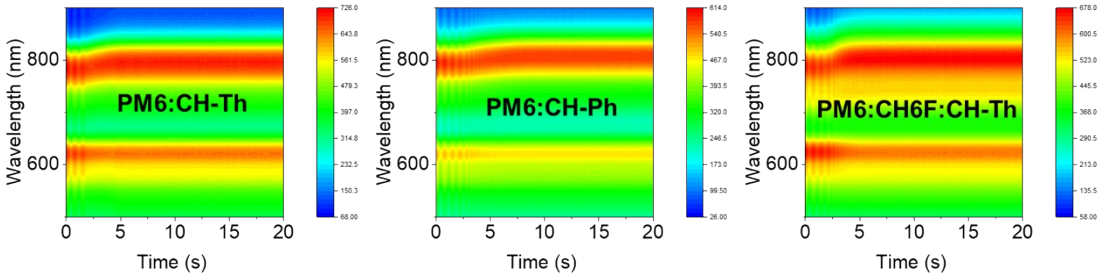

Figure S21 Color mapping of in situ UV–vis absorption spectra with thermal annealing temperature at 90 °C.

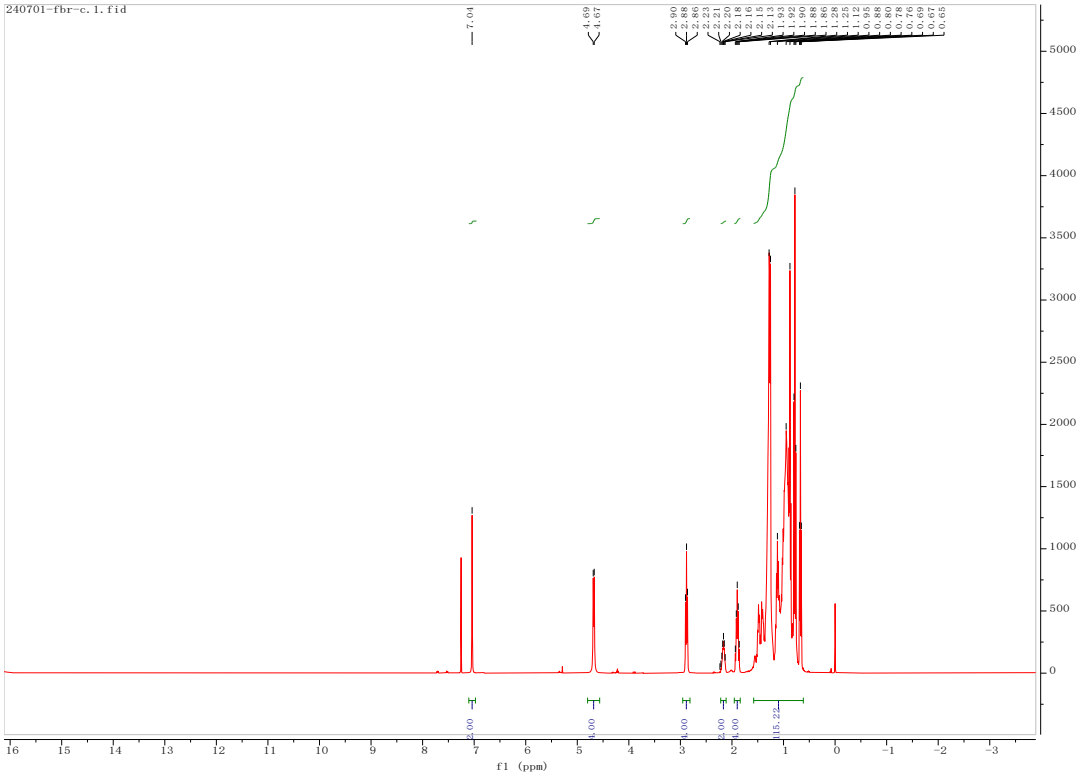

Figure S22 ^{1}H NMR spectrum of compound 2 at 300K in $CDCl_3$.

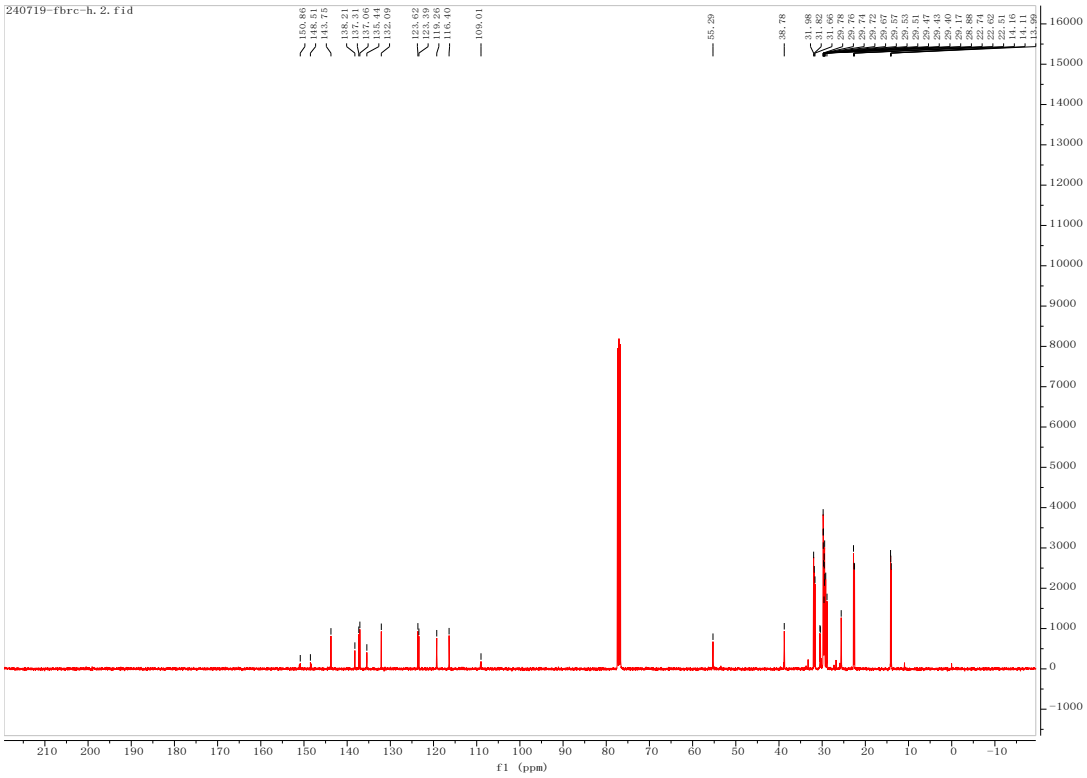

Figure S23 ^{13}C NMR spectrum of compound 2 at 300K in $CDCl_3$.

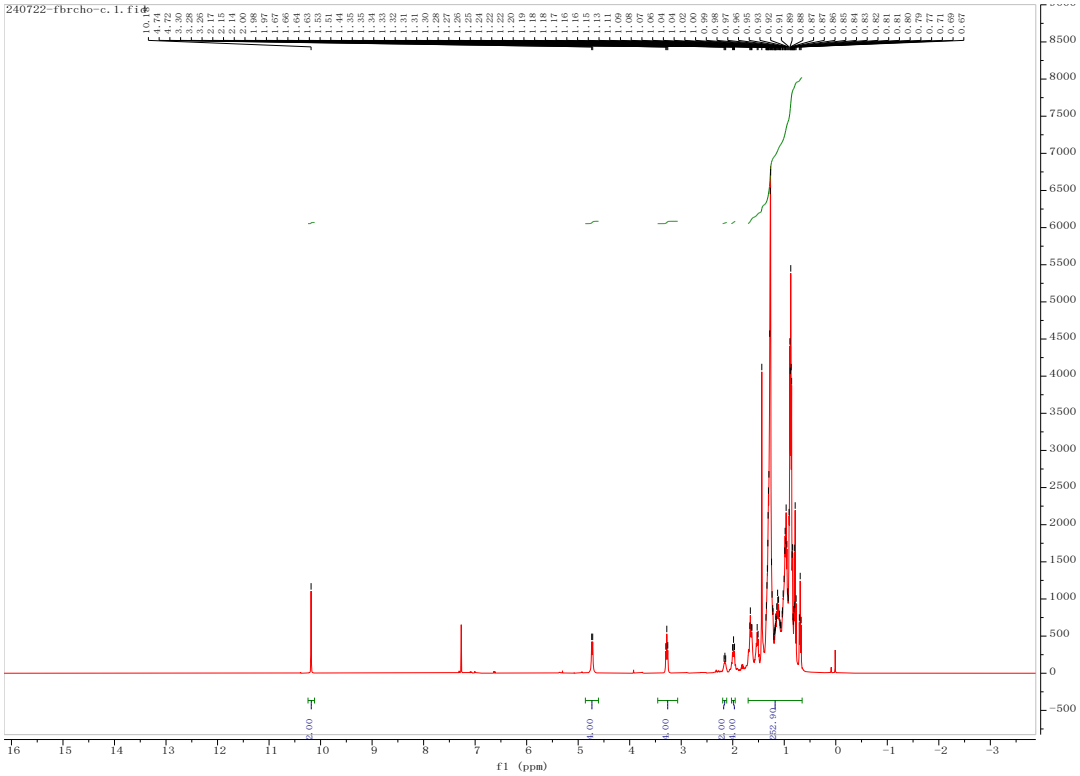

Figure S24 ^{1}H NMR spectrum of compound **3** at 300K in $CDCl_3$.

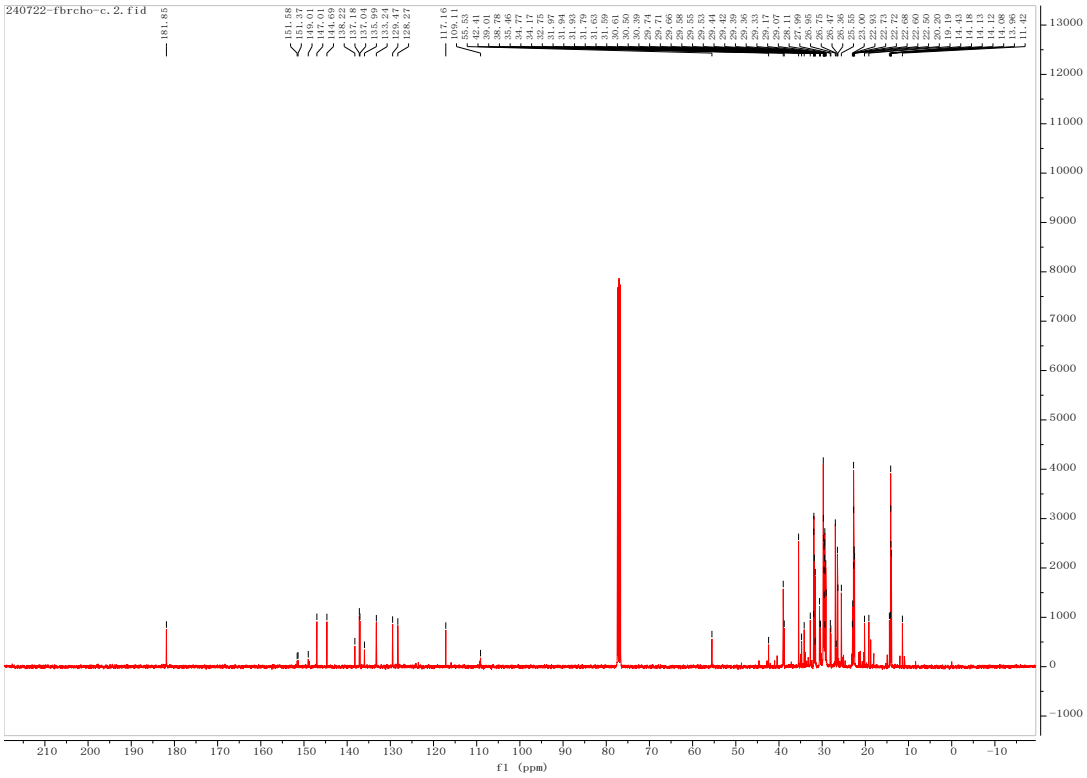

Figure S25 ^{13}C NMR spectrum of compound **3** at 300K in $CDCl_3$.

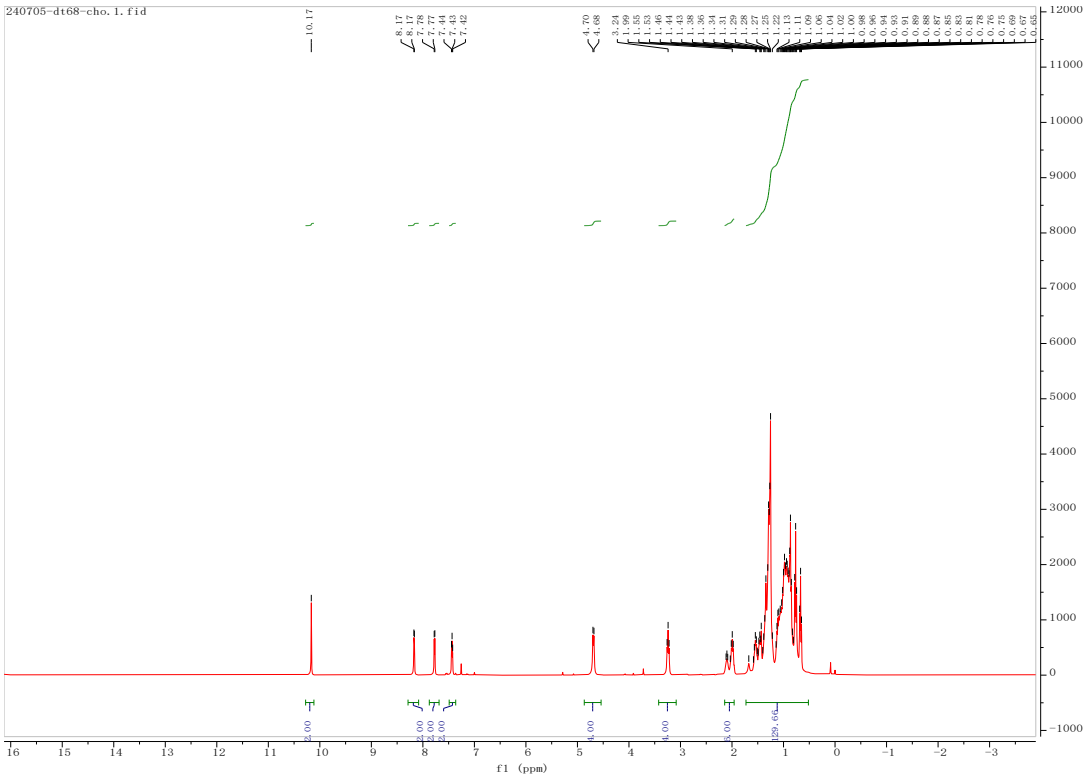

Figure S26 ^{1}H NMR spectrum of compound **4** at 300K in $CDCl_3$.

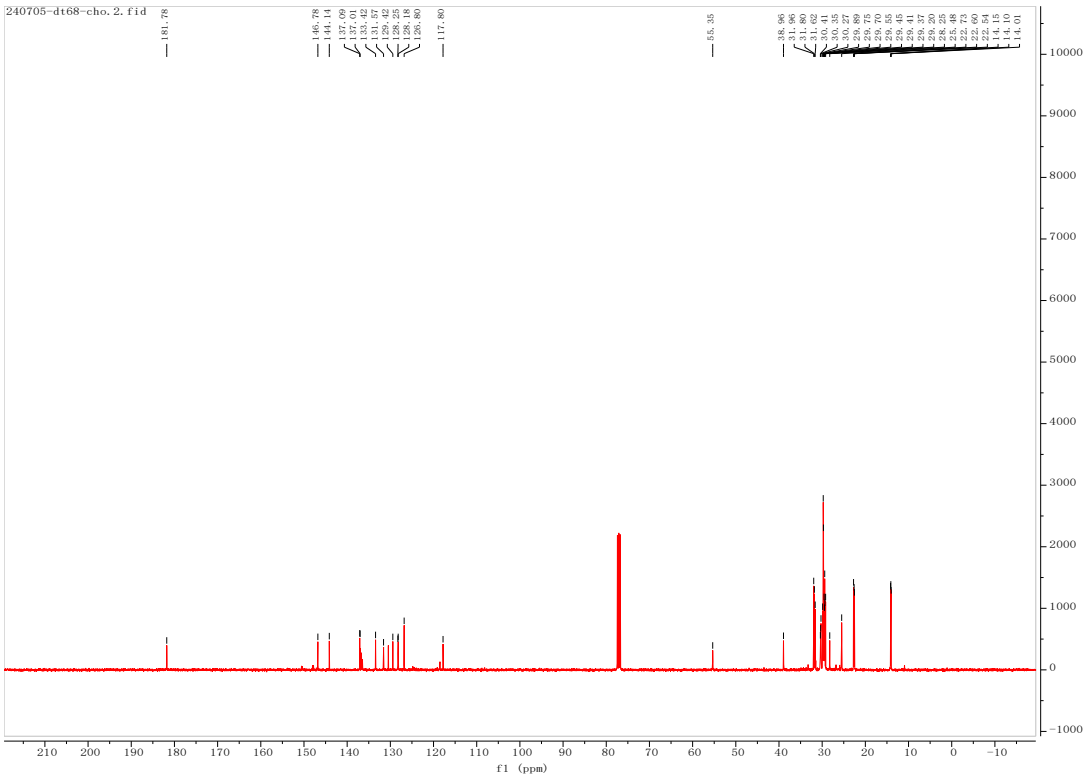

Figure S27 ^{13}C NMR spectrum of compound **4** at 300K in $CDCl_3$.

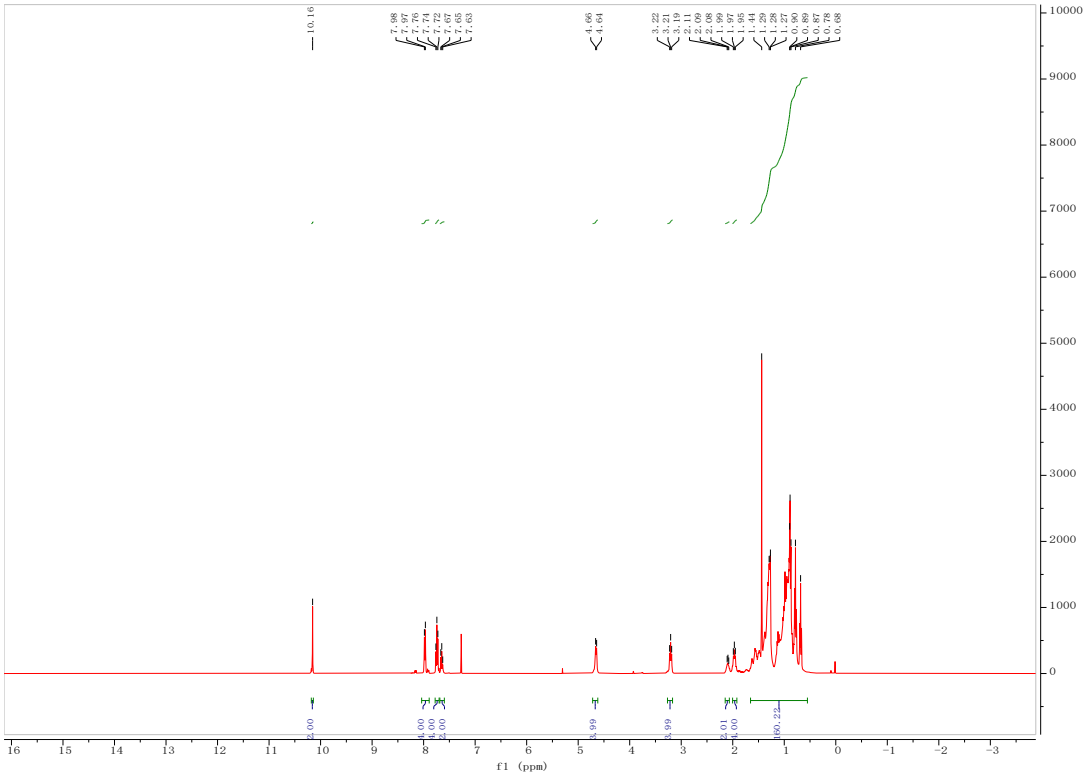

Figure S28 ^{1}H NMR spectrum of compound **5** at 300K in $CDCl_3$.

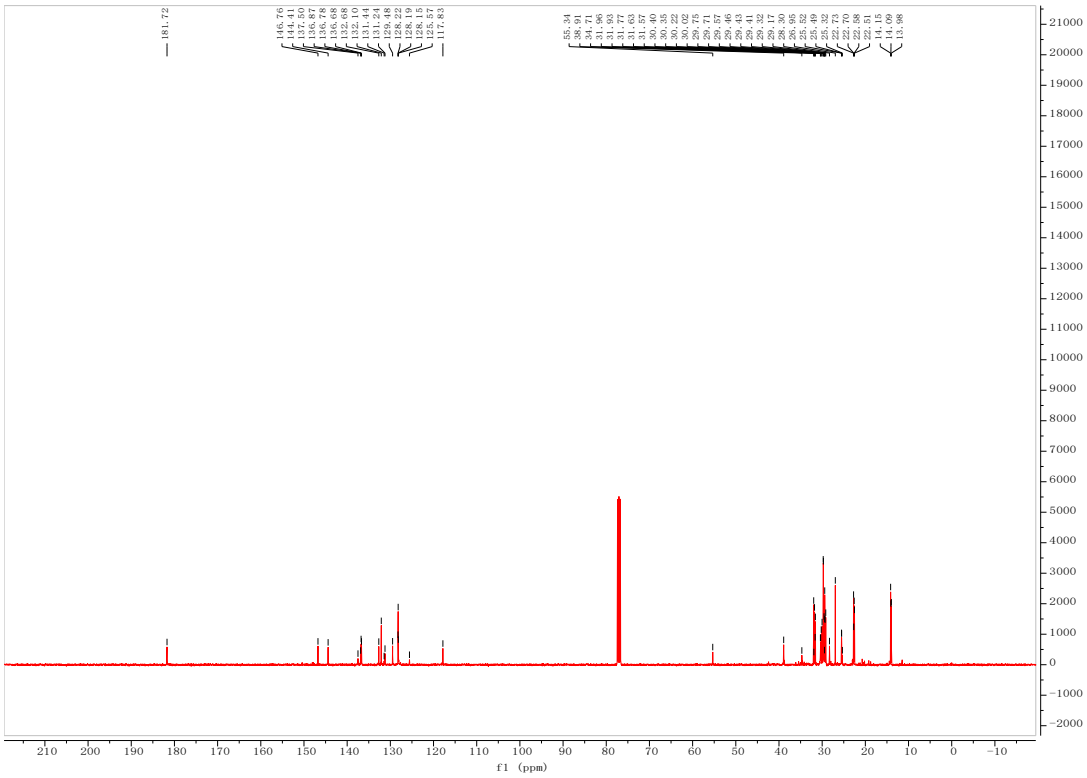

Figure S29 ^{13}C NMR spectrum of compound 5 at 300K in $CDCl_3$.

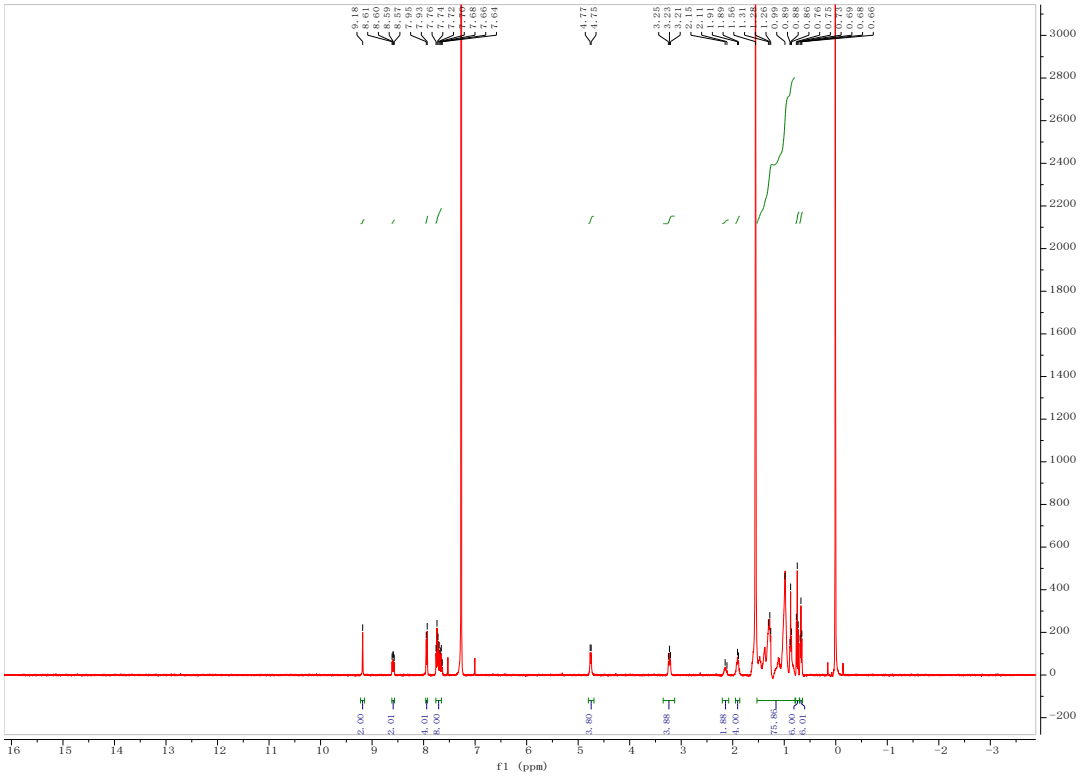

Figure S30 ^{1}H NMR spectrum of CH-Ph at 300K in $CDCl_3$.

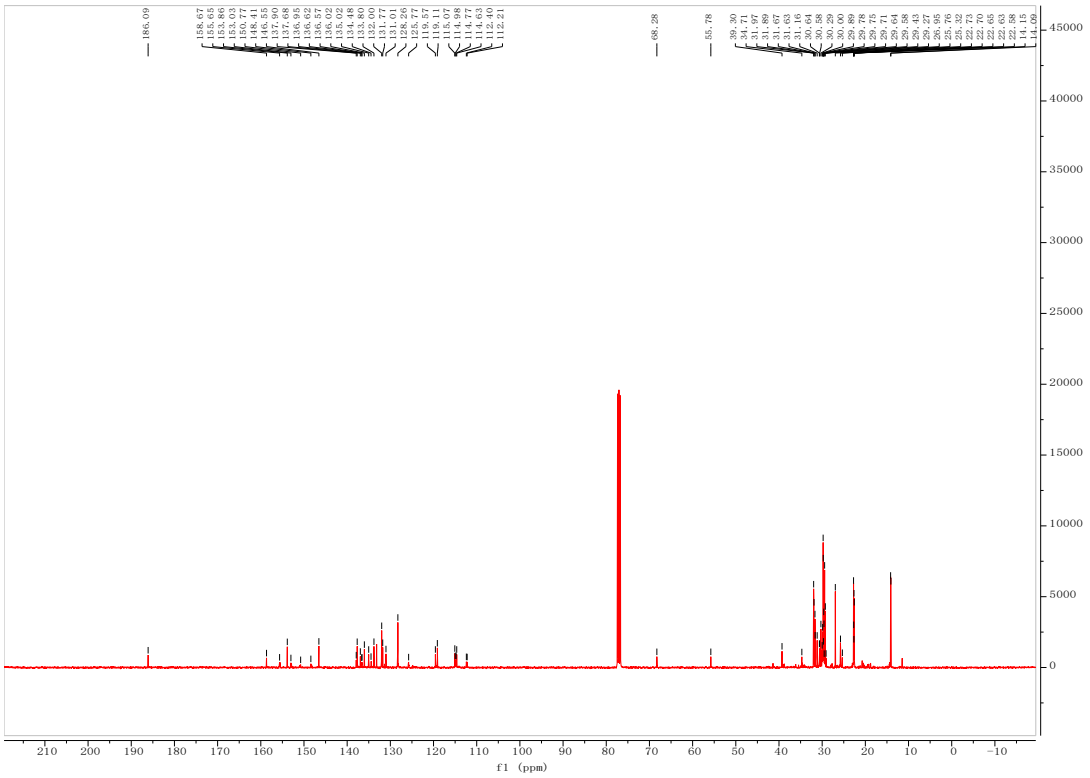

Figure S31 ^{13}C NMR spectrum of CH-Ph at 300K in $CDCl_3$.

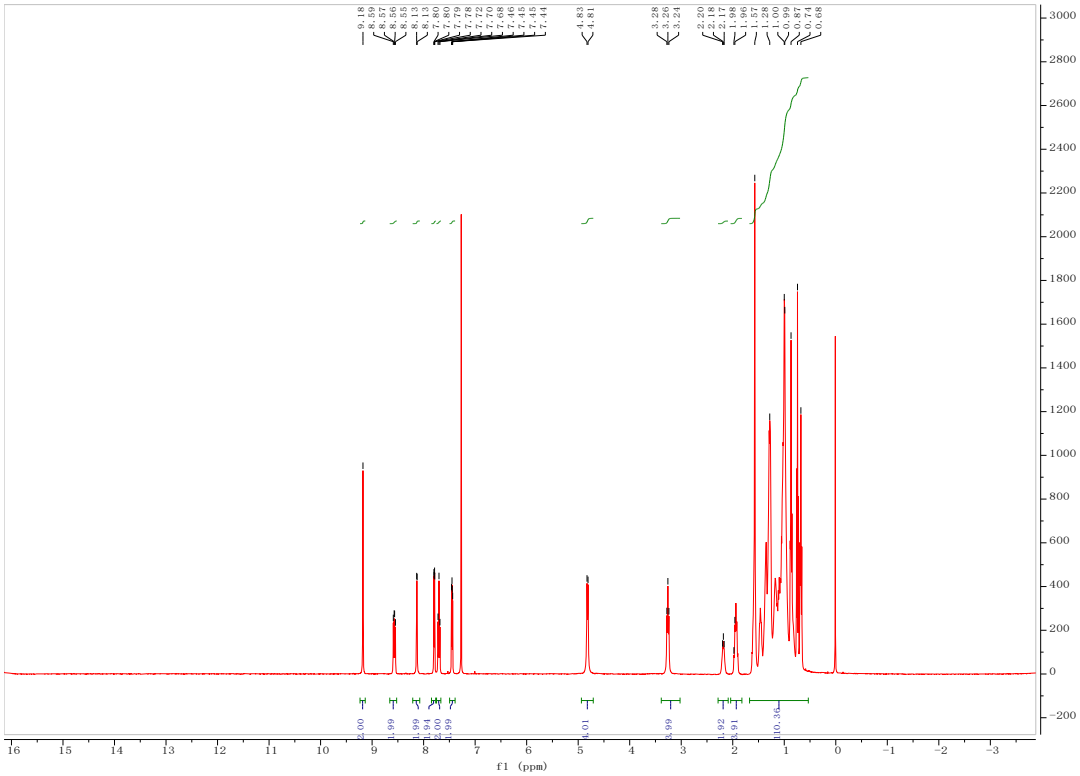

Figure S32 ^{1}H NMR spectrum of CH-Th at 300K in $CDCl_3$.

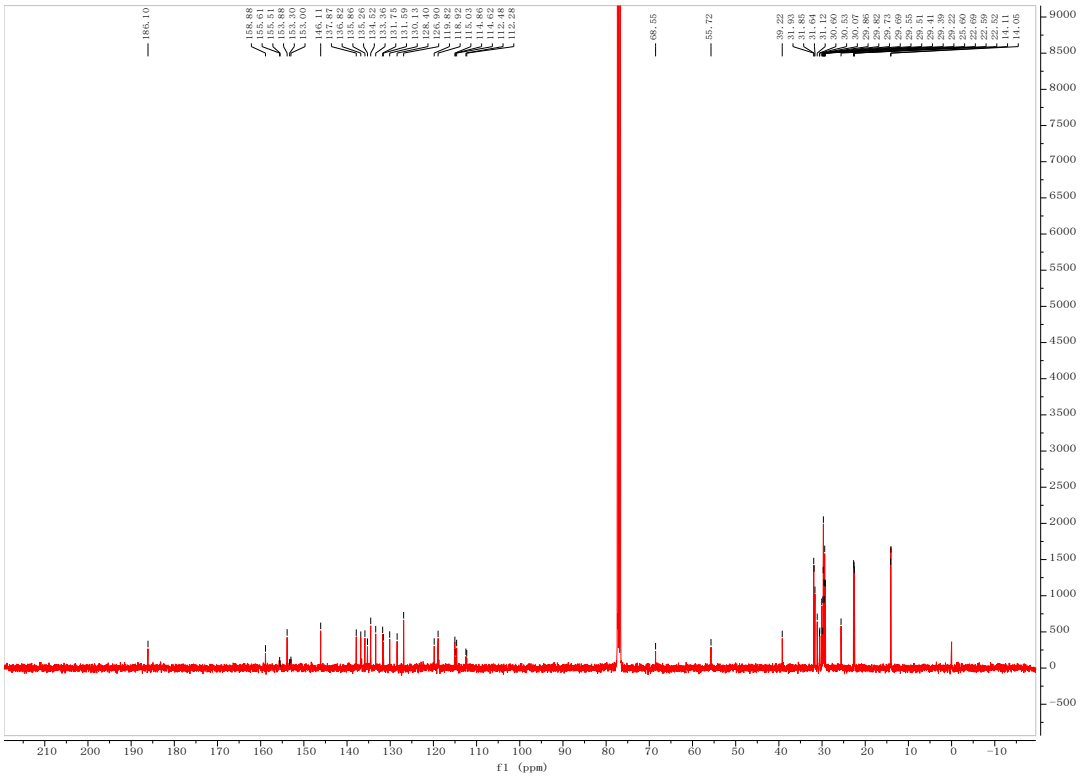

Figure S33 ^{13}C NMR spectrum of CH-Th at 300K in $CDCl_3$.

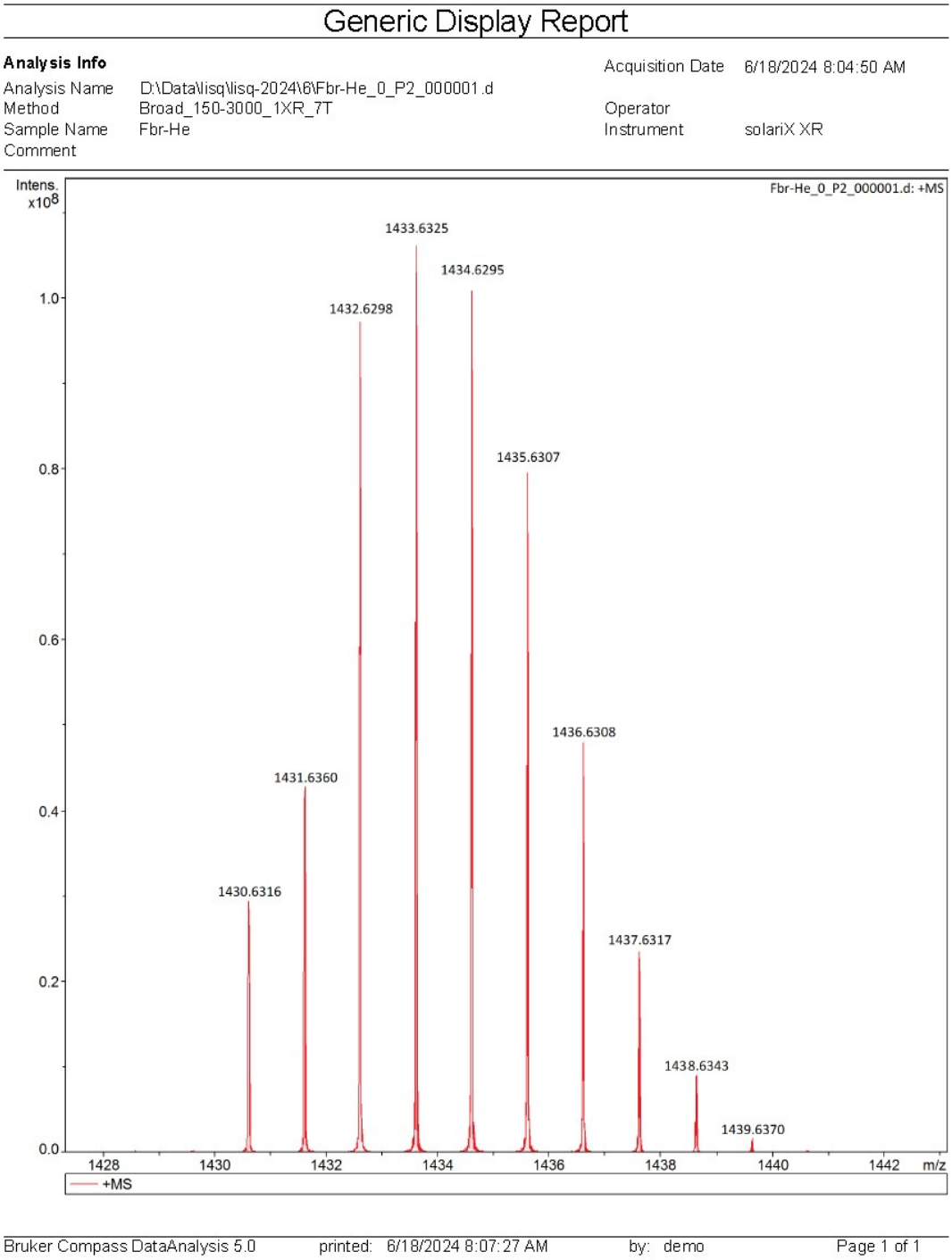

Figure S34 HR-MS of compound **2**.

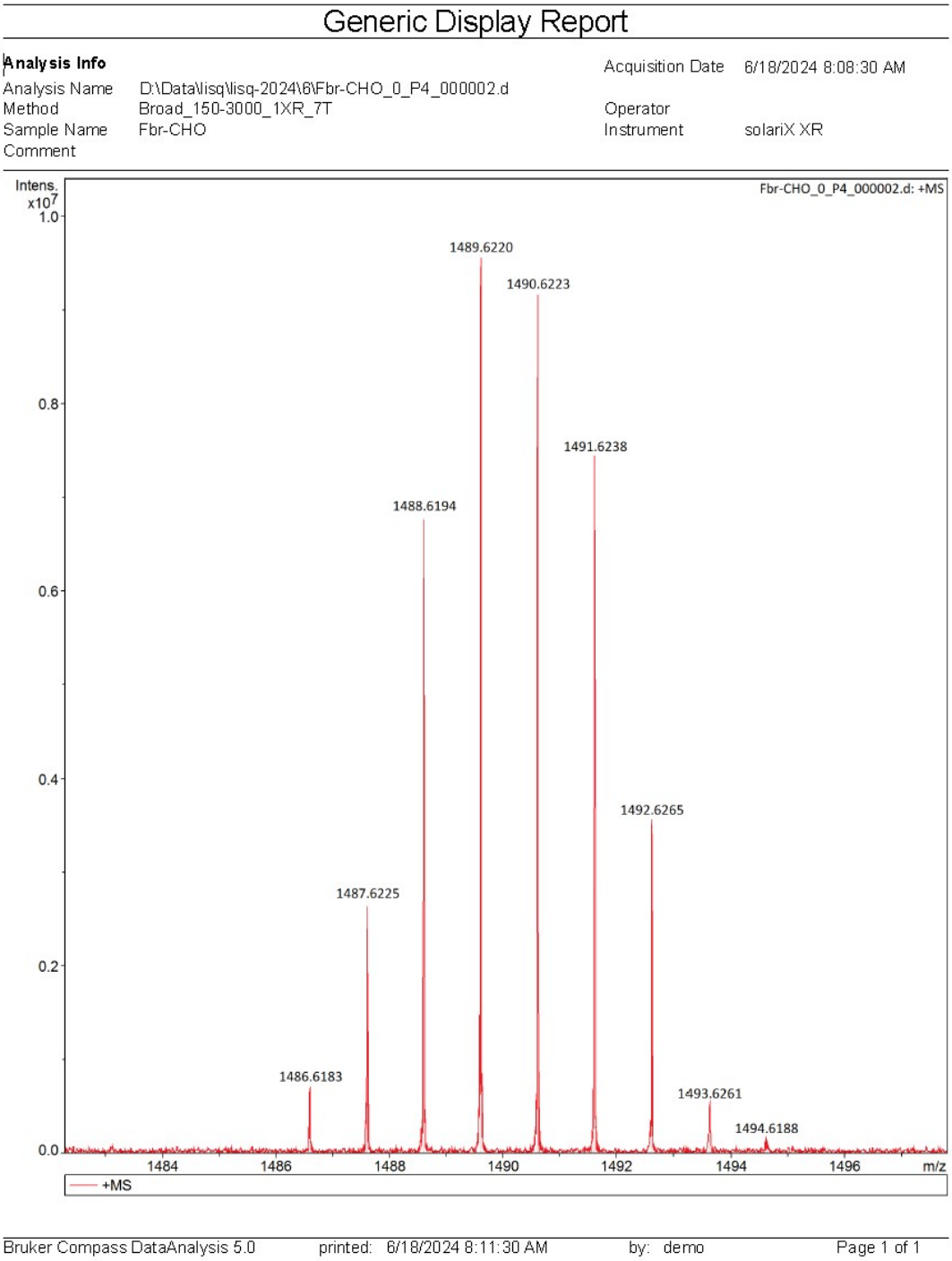

Figure S35 HR-MS of compound **3**.

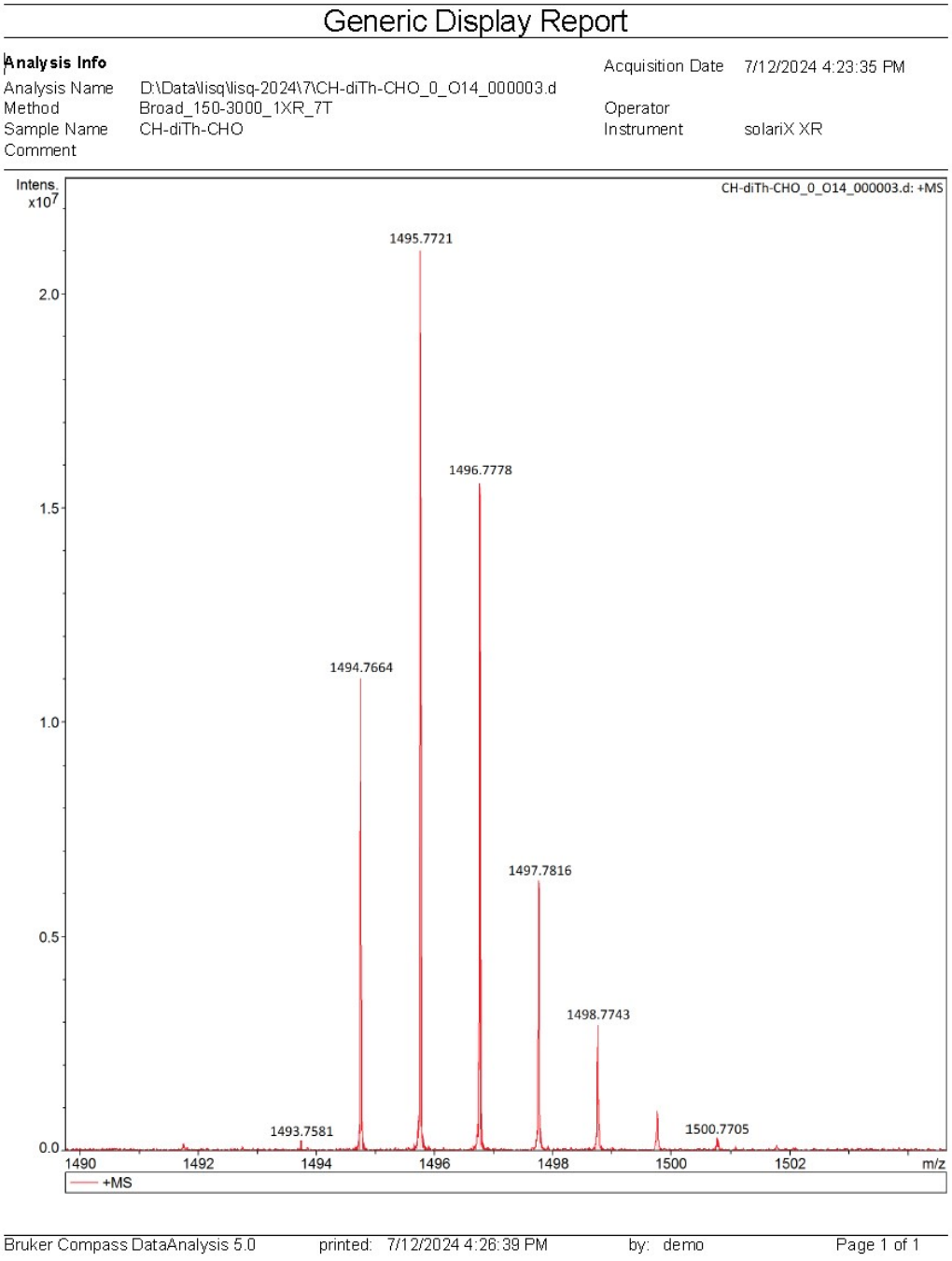

Figure S36 HR-MS of compound **4**.

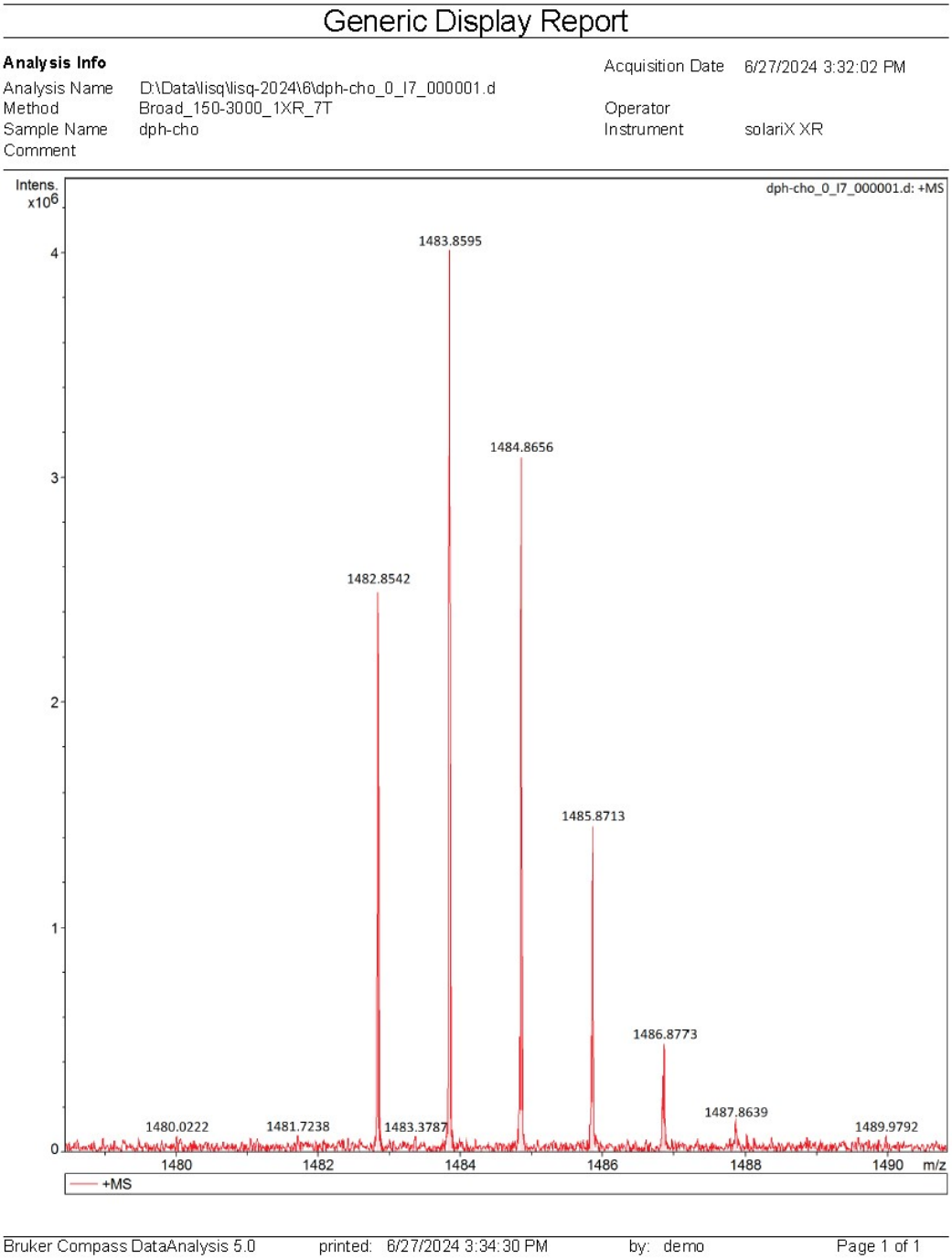

Figure S37 HR-MS of compound **5**.

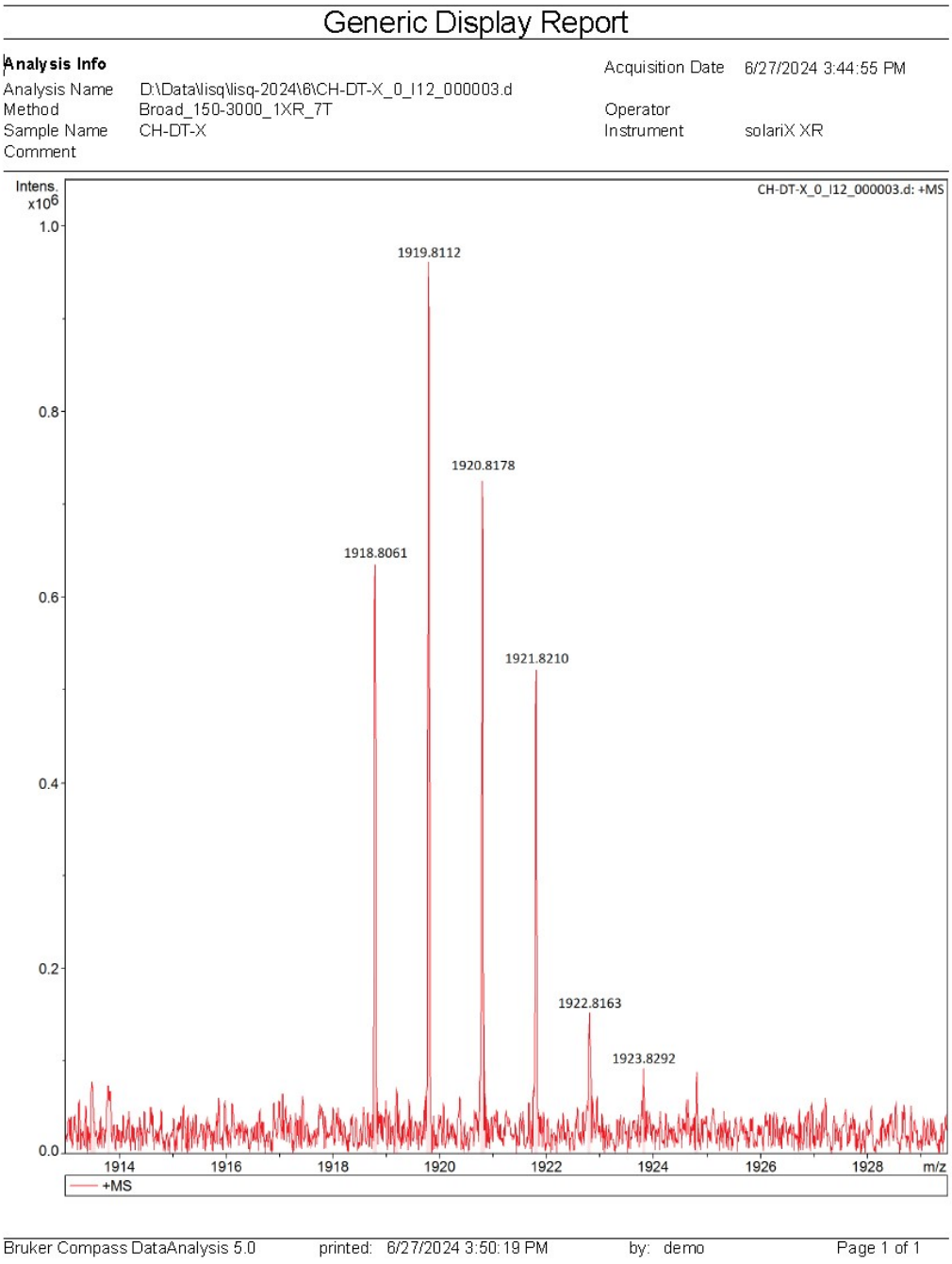

Figure S38 HR-MS of compound **CH-Th**.

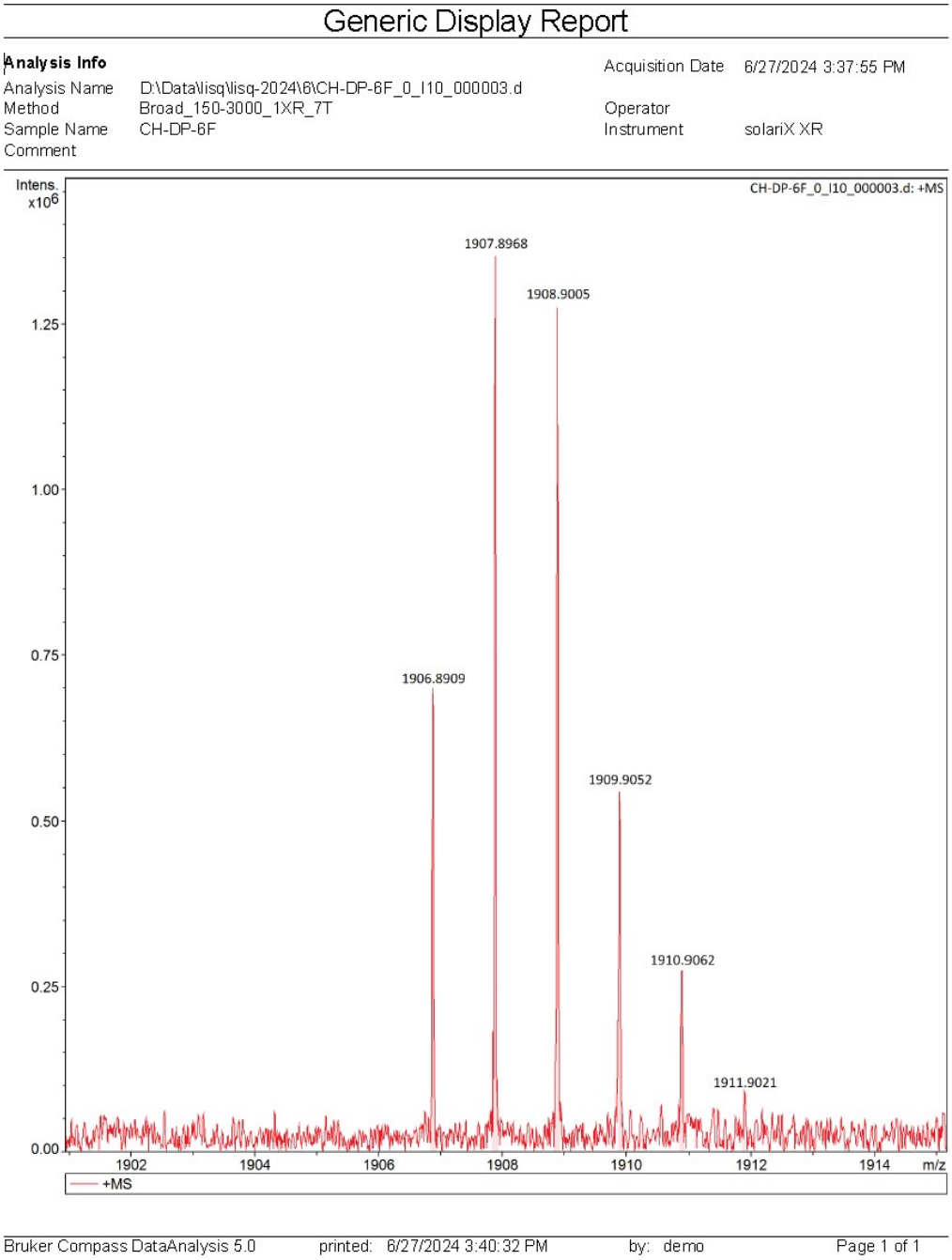

Figure S39 HR-MS of compound **CH-Ph**.

References

(1) Frisch, G.; Robb, J.; Nakatsuji, M. C.; Sonnenberg, M.; Farkas, J. B. F.; al., e. *Gaussian 16, Gaussian, Inc: Wallingford, CT,* **2016**.
(2) Becke, A. D. *J. of Chem. Phys.,* **1993**, *98* (7), 5648-5652.
(3) Hariharan, P. C.; Pople, J. A. *Mol. Phys.,* **1974**, *27* (1), 209-214.
(4) Ji, J.; Zhu, L.; Xiong, X.; Liu, F.; Liang, Z. *Adv. Sci.,* **2022**, *9* (21), 2200864.
(5) Zou, Y.; Chen, H.; Bi, X.; Xu, X.; Wang, H.; Lin, M.; Ma, Z.; Zhang, M.; Li, C.; Wan, X.; et al. *Energy Environ. Sci.,* **2022**, *15* (8), 3519-3533.